UNIVERSITÀ DEGLI STUDI DI PADOVA

Dipartimento di Fisica e Astronomia "Galileo Galilei"

Master Degree in Physics

Final Dissertation

Locked modes and plasma rotation in JET plasmas

Thesis supervisor

Prof./Dr. Lidia Piron

Candidate

Alessandra Tonel

Academic year 2023/2024

Abstract

In magnetic fusion devices, locked modes can result from the slowing down of neoclassical tearing modes (NTMs), a class of resistive magneto-hydro-dynamic instabilities that break and reconnect the magnetic field lines, or they can be induced by externally applied magnetic field perturbations. In both the cases, a magnetic island forms, which slows down plasma rotation, induces particle and energy losses, thus confinement degradation, frequently leading to a disruption. This event needs to be avoid in disruption-adverse devices, such as ITER and DEMO.

In this Thesis project, an investigation of the dynamics of locked modes has been accomplished in the Joint European Torus (JET) tokamak, located at the Culham science center (CCFE), United Kingdom. The locked mode has been induced by external 3-D fields, which have been applied by means of the Error Field Correction Coils (EFCCs). The study has been carried out at low rotation plasma regime, which is an ITER relevant regime. Data has been collected in 2023, in particular rotation measurements have been performed both during and after error field identification studies.

This Thesis project aims to investigate the behaviour of the plasma rotation in presence of externally induced locked modes and to assess strategies to stabilize them.

Contents

Chapter 1

The Magnetic Confinement of Fusion Plasmas

This chapter summarizes the physics of fusion reactors based on the magnetic confinement, exploring both the theoretical framework and the main technological methods to handle with a thermonuclear plasma. The concept of the most used fusion reactor prototype, i.e. the tokamak, is presented, together with an issue of great concern that affects this device: the magnetic instabilities. The need for investigating such kind of problems motivated this Thesis project.

1.1 Technology of Thermonuclear Fusion

One of the greatest challenges of the contemporary society is to find a balance between the increasing demand for energy and the damage caused by human activities to the environment. Human emissions of greenhouse gases while burning fossil fuels are one of the main driver of the climate change. Moreover, carbon fuels do not represent a renewable source of energy and they are not homogeneously spread all over the world, which is a motive of geopolitical tensions. Nowadays, two emission-free sources of energy are available, i.e. renewable sources and nuclear fission, but they have to face other problems. On one hand, renewable energies (solar, wind, hydroelectric, geothermal) are characterized by an aleatory output and they can not be used for baseline production. On the other hand, the disadvantage of nuclear fission energy is the managing of the long-lived radioactive byproducts (several thousands of years).

As it will be clear in Subsection 1.1.3, fusion energy would be the perfect solution, since it would represent a clean, large-scale sustainable, reliable and carbon-free energy source. These intrinsic properties have motivated scientists and engineers to carried out research on fusion technology since the '50s.

1.1.1 Thermonuclear fusion reaction

All stars are plasmas self-sustained by nuclear fusion reactions between light nuclei, that are converted into a heavier one: for example, in our Sun hydrogen nuclei fuse into a nucleus of Helium during the so called *p-p chain*, that happens in its core, where critical conditions of temperature and pressure are found ($T \sim 15 \times 10^6$ K, $P \sim 5 \times 10^{11}$ atm). In nature, nuclear fusion occurs spontaneously in the left part of the plot reported in Figure 1.1, which represents the binding energy per nucleon as a function of the nucleus mass number. Hence, for these light nuclei, the reaction leads to a gain in the final binding energy, which means a defect of the mass energy that follows Einstein's relation, $E = mc^2$, that is released as kinetic energy of the final products. The aim of a thermonuclear fusion reactor is to convert this kinetic energy

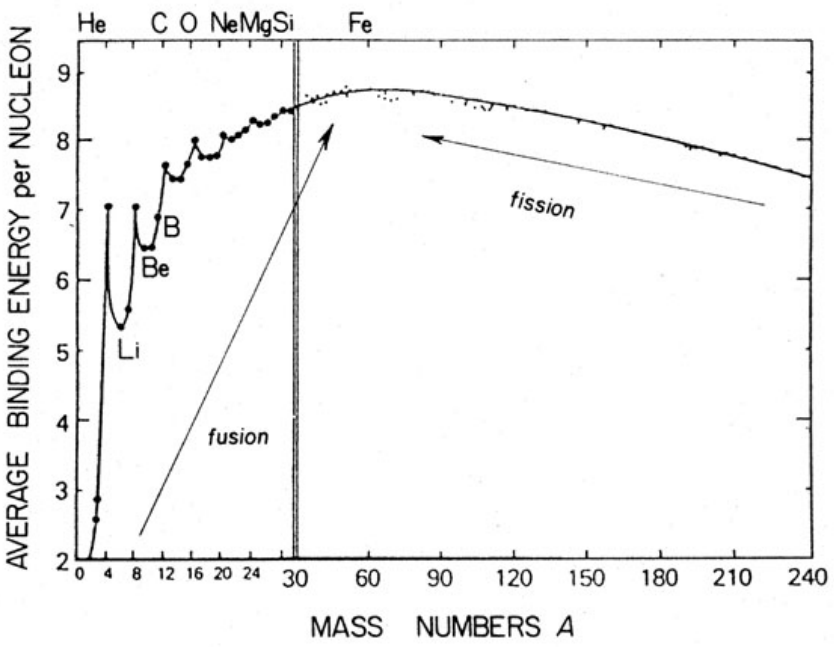

Figure 1.1: Plot of the mean binding energy per nucleon as a function of the mass number. Nuclear fusion and fission reactions occur spontaneously for nuclei, respectively, below and after the so called *iron peak* (A∼55). Peaks in the binding energy in the left side of the plot are due to shell effects (magic and double magic nuclei).

into electricity to be used for human society. If we could emulate the Sun's processes in human laboratories, we could use light nuclei widely spread on Earth as a basically inexhaustible fuel to achieve a high, clean and sustainable production of energy.

As it has been anticipated, a star is a plasma, which is considered the fourth state of matter and consists in an ionised gas in which at least one atomic bond has been broken, leaving a free electron and a positively charged nucleus known as ion. The high temperatures of stars are responsible for these breaks and, in particular, they are such high that all the atomic electrons are freed from the nuclei. While in the sun the massive gravitational force naturally induces the fusion, without that force a temperature even higher is needed for the reaction to take place. On Earth, a thermonuclear plasma must be realized and particles within it must be kept in a confined region for a time much longer than the collision time. Temperatures of over one hundred million of Celsius must be reached, in order to make possible the overcoming of the Coulomb barrier that develops between the charged ions in the plasma. In fact, Coulomb scattering cross section is generally higher than fusion cross section and such events would cause an unsustainable loss of particles and energy, if a simple fixed-target experiment were chosen. Two main methods can be used to confine a plasma:

- the *magnetic confinement* exploits a magnetic field to bend the trajectories of the plasma particles in the perpendicular plane, therefore creating circular orbits around the field lines. They are characterized by a Larmor curvature radius, $\rho_{Lar} = \frac{mv}{qB}$, where m, v and q are respectively the mass, the velocity and the charge of the particle and B is the magnetic field;

- the *inertial confinement* exploits a target made of solid pellets of the nuclei interested in the reaction, that is heated up by a high power laser or heavy ion beams. This brings to the vaporization of the external layer of the target, that drives a compression on the inner part, leading to a strong increase of the density, through which the overcoming of the Coulomb barrier becomes possible.

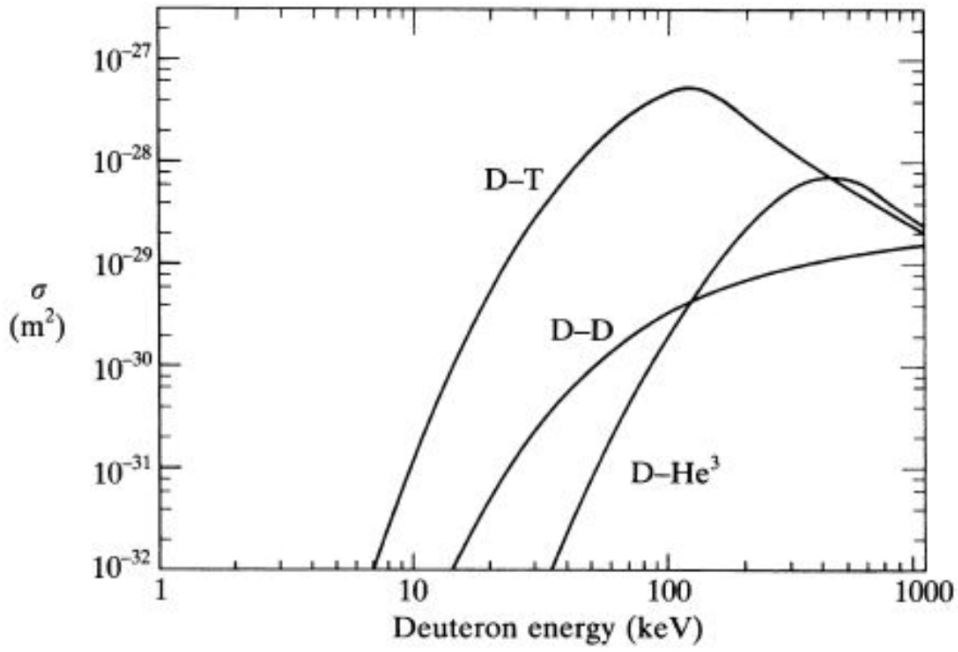

Figure 1.2: Plot of the cross sections for the main fusion reaction candidates as functions of the kinetic energy of the incoming particle, evaluated in the reference frame in which the target particle is stationary.

The European Fusion Programme is based on the magnetic confinement.

For technological purposes, Hydrogen isotopes, mainly Protium (H), Deuterium (D) and Tritium (T), are the best candidates, for which the main fusion reactions are:

$$\begin{aligned} {}^2\mathrm{D} + {}^2\mathrm{D} &\longrightarrow {}^3\mathrm{He} + {}^1\mathrm{n} + 3.27\ \mathrm{MeV} \\ {}^2\mathrm{D} + {}^2\mathrm{D} &\longrightarrow {}^3\mathrm{T} + {}^1\mathrm{H} + 4.03\ \mathrm{MeV} \\ {}^2\mathrm{D} + {}^3\mathrm{T} &\longrightarrow {}^4\mathrm{He} + {}^1\mathrm{n} + 17.6\ \mathrm{MeV} \\ {}^2\mathrm{D} + {}^3\mathrm{He} &\longrightarrow {}^4\mathrm{He} + {}^1\mathrm{H} + 18.3\ \mathrm{MeV} \end{aligned} \tag{1.1}$$

This comparison would suggests that the last reaction is the preferable one, since the released energy is the highest, however, it is also important to consider the cross section values in the energy range of interest (10-20 keV in our case, see Subsection 1.1.4). The evidences depicted in Figure 1.2 show that the third reaction, i.e. the one between D and T, is characterized by the highest cross section. For this reason, it is the most suited to be exploited in fusion reactors, despite the disadvantage of using Tritium, since it is an unstable nucleus that $\beta-$decays with an half life of only 12.3 years.

1.1.2 The concept of a fusion reactor

While Deuterium is stable and can be extracted from all forms of water, Tritium must be bred in the fusion machine itself, by exploiting reactions of the neutrons produced by the D-T fusion with Lithium. This is achieved in the first layer external to the plasma vessel, that is called the *breeding blanket*. The two n-Li reactions of interest are the following:

$$\begin{aligned} {}^6\mathrm{Li} + {}^1\mathrm{n} &\longrightarrow {}^4\mathrm{He} + {}^3\mathrm{T} + 4.8\ \mathrm{MeV} \\ {}^7\mathrm{Li} + {}^1\mathrm{n} &\longrightarrow {}^4\mathrm{He} + {}^3\mathrm{T} + {}^1\mathrm{n} - 2.5\ \mathrm{MeV} \end{aligned} \tag{1.2}$$

Fast neutrons (14.1 MeV) emitted in the fusion react with ^{7}Li de-accelerating, thus becoming slow neutrons that are absorbed by ^{6}Li. The released energy is converted into heat, which

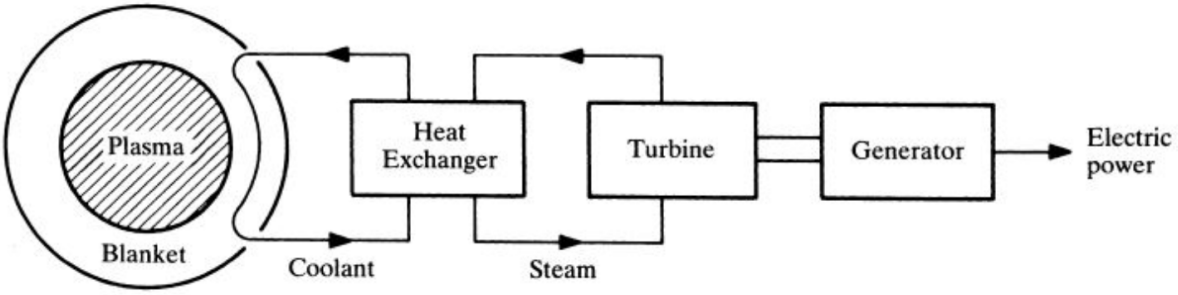

Figure 1.3: Scheme of a thermonuclear fusion power plant.

causes the production of steam that activates a turbine for the electricity production: this is the essential principle of a fusion power plant, which is depicted in Figure 1.3. A further advantage of the breeding blanket is that, because a great fraction of the neutrons is absorbed, the external materials are highly shielded from neutron radiation. The two reactor fuels are thus Deuterium and Lithium, which is an abundant element in the Earth's crust.

1.1.3 Advantages of fusion energy

Deuterium and Lithium supplies would last for millions of years, making fusion energy basically inexhaustible. Other advantages against the other sources are the following:

- 10 g of D and 30 g of Li (to produce 15 g of T) are enough to supply energy for the lifetime of an average person in an industrialised country;
- the releases energy is about one million times the energy produced with chemical reactions (burning of fossil fuels) and four times the energy emitted in nuclear fission reactions at equal mass. Fusion has the potential to provide a baseload of electricity for our cities and industries;
- the considered fusion reaction produced Helium, an inert and harmless gas, and neutrons that potentially can activate the power plant structure, but practically this activation decays rapidly (hundred of years) and the time span before it can be utilized again can be minimised by selecting low-activation materials;
- no risk of meltdown nor run away uncontrolled production of energy are possible, since it is difficult to reach and maintain the conditions necessary for fusion. If any disturbance occurs, the plasma cools down within seconds and the reactions stop.

1.1.4 Power balance equation

In contrast to neutrons, α particles, being charged, are confined by the magnetic field in the plasma and release their kinetic energy by elastic scattering with the plasma particles, until they are thermalized. Hence, they represent an intrinsic source of heat in the plasma, which contributes in giving the sufficient energy to D and T ions to make the fusion possible. However, an external source of heat is needed to create the proper thermal environment, since the pure Ohmic heat is not sufficient for reaching the required temperature.

The *power balance equation* is the equilibrium relation between all the power terms that increase or decrease the plasma thermal energy:

$$\frac{\mathrm{d}w}{\mathrm{d}t} = p_\alpha + p_H - p_L - p_{rad}. \tag{1.3}$$

In Equation 1.3, w represents the plasma thermal energy density, that is, according to the kinetic theory of gases, $w = 3nT$, for a plasma at a temperature T, with a density of electron and ions both equal to n. Its variation in time, $\frac{\mathrm{d}w}{\mathrm{d}t}$, is given by the gain terms p_α and p_H, that are, respectively, the power released by the α particles and the external heat contribution, and by the losses p_L and p_{rad}, where the former originates from transport processes, while the latter includes all the radiative emissions from the plasma.

From the kinematics of nuclear reactions, α particles carry $\frac{1}{5}$ of the total power released by the fusion, that is

$$p_f = n_D n_T \langle \sigma v \rangle_T E_f = \frac{1}{4} n^2 \langle \sigma v \rangle_T E_f, \tag{1.4}$$

where n is the density of a plasma made of 50% of D and 50% of T, $E_f = 17.6$ MeV is the total energy released by the fusion reaction and $\langle \sigma v \rangle_T$ represents the *reactivity*, which is a quantity related to the reaction count rate:

$$R = n_D n_T \langle \sigma v \rangle_T. \tag{1.5}$$

It is a function of the temperature and, in particular, in the temperature range of interest is well approximated by

$$\langle \sigma v \rangle_T = 1.1 \times 10^{-24}\ T^2\ m^2 s^{-1}. \tag{1.6}$$

The radiative term consists in three contributions: 1) the line emissions that follow the excitation of bound electrons in partially ionized atoms; 2) the cyclotron radiation due to the gyration motion of the charged particles that compose the plasma; 3) the Bremsstrahlung emission, that originates from the change in the velocity of the charged particles, electrons in particular, due to collisions, in presence of the nuclear field of D and T ions. The latter is the dominant process, since the second one is usually negligible and the first one is zero for thermonuclear plasmas, where atoms are fully ionized. Therefore

$$p_{rad} \sim p_B = a_B n^2 \sqrt{T}\ W m^{-3} \tag{1.7}$$

is a good approximation, with $a_B = 5.35 \times 10^{-37}\ W m^3 keV^{-\frac{1}{2}}$. However, the contribution given by (1) can increase in presence of neutral impurities, whose electrons can be either excited or extracted from the atoms by collision events.

The transport loss term is the most difficult to describe theoretically. It is in general defined as

$$P_L = \frac{W}{\tau_E}, \tag{1.8}$$

where W is the plasma thermal energy and τ_E is the *energy confinement time*, which is one of the main operative parameters to take into account when a thermonuclear fusion device is built. In absence of any external heating power, if the α particles contribution and the radiative emissions are negligible, by combining Equations 1.3 and 1.8, it results that the energy confinement time is the characteristic time of the exponential drop of the plasma energy due to transport losses:

$$w(t) = w_0 e^{-\frac{t}{\tau_E}} \tag{1.9}$$

It is thus a measure of how long the energy in the plasma is retained before being lost: the larger is τ_E, the better is the confinement.

The *triple product*, $nT\tau_E$, is the product between the three main quantities that characterized a thermonuclear plasma, since, as mentioned above, in fusion devices the plasma must be dense, hot and confined. Let us consider the stationary regime ($\frac{\mathrm{d}w}{\mathrm{d}t} = 0$) and the so called *ignition condition*, that is reached when the plasma is self-sustained, i.e. the fusion reactions happen only

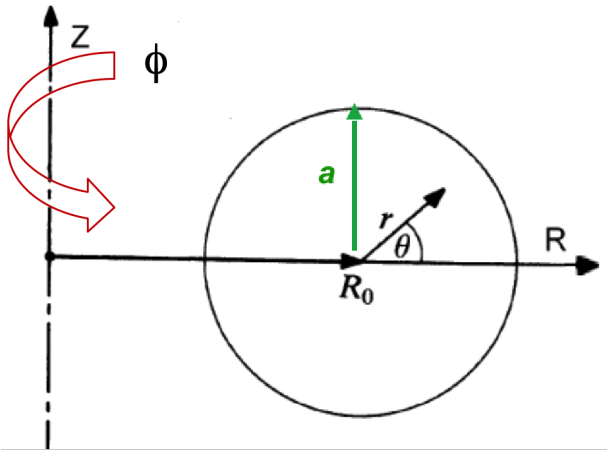

Figure 1.4: Toroidal coordinates.

thanks to the energy released by α particles ($p_H = 0$). If p_{rad} is negligible and the definition of reactivity in Equation 1.6 is used, a lower limit for the triple product is found:

$$nT\tau_E > 3 \times 10^{21}\ m^{-3} keV s \tag{1.10}$$

Realistically, this is fulfilled, for example, by the following values

$$\begin{cases} n \sim 1 - 2 \times 10^{20}\ m^{-3} \\ T \sim 10 - 20\ keV \\ \tau_E \sim 4 - 6\ s \end{cases}, \tag{1.11}$$

that are the ones used in most of the present fusion experiments.

Although the ignition condition could seem advantageous, it is more convenient to have an active control on the plasma, which is obtained by exploiting external heating sources. P_H is in fact a quantity controlled by the operator. In any case, in order to obtain a positive gain of energy from the reactor, the quantity $Q = \frac{P_f}{P_H}$ must be greater than 1, i.e. the output power must overcome the input one.

1.2 Tokamaks

Nowadays, the geometry mostly employed in the building of fusion machine experiments is the torus, a sort of closed cylinder, because it allows the possibility to close the magnetic field lines ideally preventing particle losses and leading, in this way, to the best confinement configuration. In particular, a toroidal fusion device that exploits the magnetic confinement is called *tokamak*, a word that is the result of the combination of two Russian expressions: *toidalnaya kamera* (toroidal chamber) and *magnitnaya katushka* (magnetic coil). The toroidal coordinates, (R, Z, ϕ), are represented in Figure 1.4: the ϕ coordinate, called the *toroidal direction*, represents the magnetic axis and refers to the direction along which a cylinder is closed to form a torus, while the (R,Z) plane is orthogonal to ϕ and it is called *poloidal plane*. In tokamaks the magnetic field in the toroidal direction, B_ϕ, is created by external coils placed all around the torus in the poloidal plane. Because of the non uniformity of this field ($B_\phi \propto \frac{1}{R}$), resulting from Ampére's law, a poloidal component, B_p, is also required to ensure the confinement. Its intensity is about one order of magnitude lower than B_ϕ and it is generated by inducing a toroidal current in the plasma itself, exploiting the transformer principle. In particular, the primary windings are represented by a solenoid put in the torus central hole, while the plasma plays the role of the

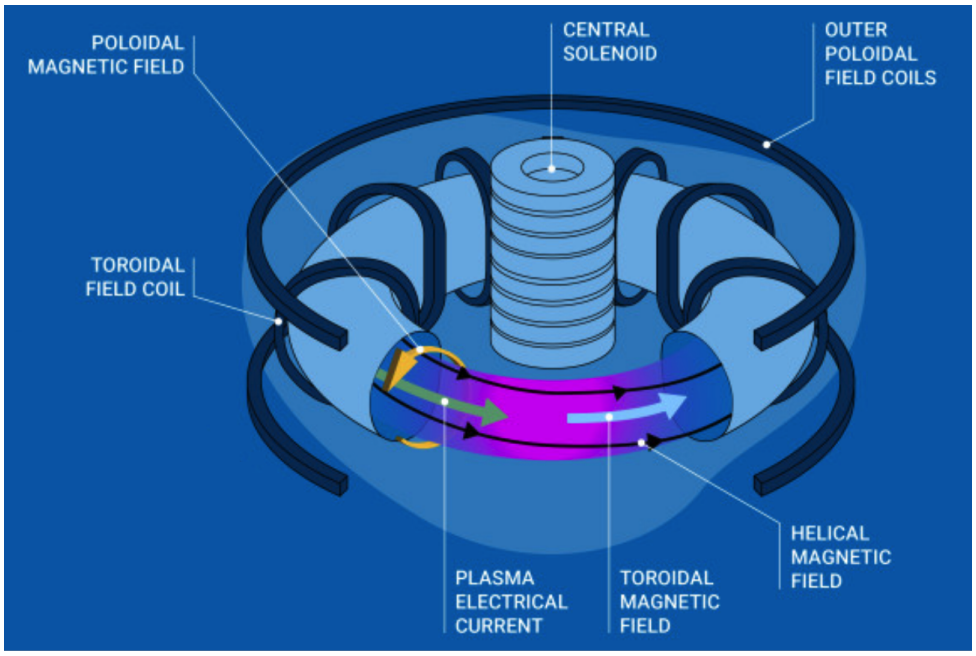

Figure 1.5: Scheme of a tokamak device.

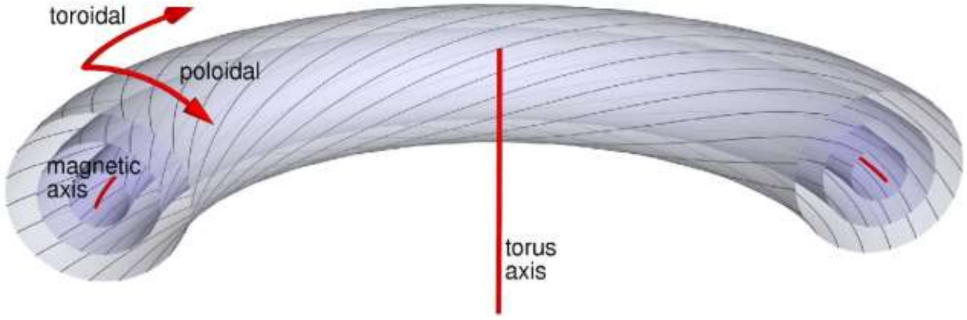

Figure 1.6: Representation of the nested magnetic field surfaces, containing the magnetic field lines.

secondary circuit. Such a device is schematize in Figure 1.5. The total magnetic field is therefore the superposition of these two contributions and its surfaces are nested in the poloidal plane (Figure 1.6), with a shape that can be varied with the external position and shape control coils (see Subsection 1.4.1). The magnetic field lines are thus closed along both the toroidal and the poloidal direction, being helices wrapped around the magnetic surfaces. The plasma particles follow a helical path around them, as shown in Figure 1.7. Magnetic field surfaces are usually described by a important figure of merit that is called *safety factor*, which is defined as the normalized toroidal angle that a magnetic field line on a certain surface must cover in order to accomplish a full poloidal turn:

$$q(r) = \frac{\Delta\phi}{2\pi} \sim \frac{rB_\phi(r)}{R_0 B_\theta(r)}, \tag{1.12}$$

where the second relation is derived from the field line equation solved in the cylindrical approximation. In a tokamak, $q(0)$ is forced to be 1 by a class of MHD instabilities (sawtooth oscillations), while it increases up to 3-4 at the plasma edge (Figure 1.14). As it will be encountered later in this Thesis, q is related to the magnetic field perturbations and thus to plasma instability, from which its name originates (see Subsection 1.4.2).

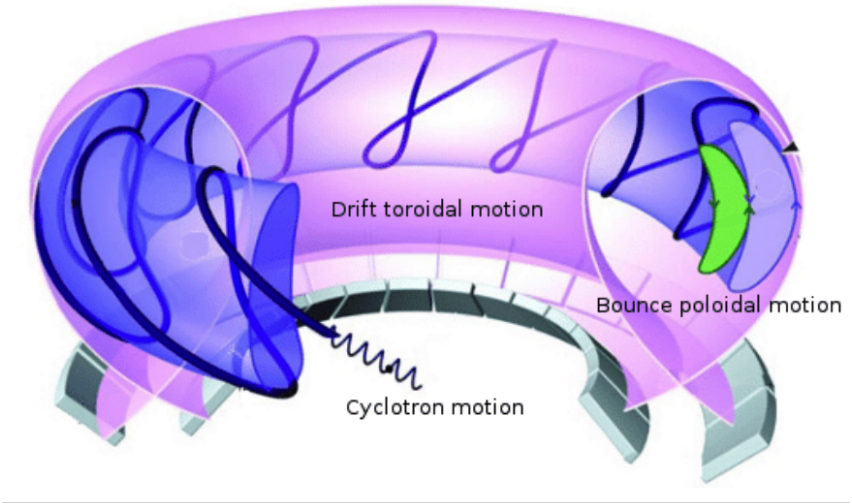

Figure 1.7: Representation of the particles trajectories along the magnetic field lines.

1.3 ITER

The tokamak concept was proposed in 1950 by the soviet scientists Andrei Sakharov and Igor Tamm. In the same year, Lyman Spitzer came out with the idea of the *stellarator*, a fusion device in which the helical field lines are realized only through the use of external coils, placed poloidally around a torus with a twisted complex geometry, such that the external current follows a sine law, $I(\theta) \propto sin(l\theta - M\phi)$, with l and M integers. Stellarators dominated the fusion research during the '50s and the '60s, then being overcome by tokamaks for their best performances.

From the collaboration of many European countries, the Joint European Torus (JET) was design in 1973 and between 1977 and 1983 it was built at Culham in Oxford, becoming the largest operational fusion experiment exploiting magnetic confinement.

In 1985 the idea of a collaborative international project on fusion energy was proposed by General Secretary Gorbachev of the former Soviet Union to US President Reagan, from which the International Thermonuclear Experimental Reactor (ITER) took origin. The project started in 1988 and the first plasma is foreseen to be ready not before 2033, while the first D-T operation will start not before 2039. Currently, it is being built in Cadarache, Southern France, and the largest economies in the world are involved in it: EU, USA, Russia, China, South Korea, Japan, India. ITER will allow to investigate many scientific and technological issues, which are beyond the present capabilities. It will be the first device routinely operating with D and T and will combine in its design the greatest achievements in fusion research, such as superconducting coils to ensure long lasting plasma discharges, Beryllium first walls and Tungsten divertor to obtain low impurity pollution and fuel retention. Its main characteristic are presented in Table 1.1 and in Figure 1.8 a sketch of the future design is depicted.

The main goals of ITER are:

- creating a D-T plasma in which the fusion conditions are achieved mostly by internal fusion heating (α particles heating);
- generating 500 MW of fusion power from 50 MW in input for long pulses ($\sim$10 minutes);
- studying plasmas under conditions similar to those expected in future power plants;
- investigating the reasons of the onset of magnetic field instabilities and testing methods to reduce them;

Parameter	Value
Major radius	6.2 m
Minor radius	2.0 m
Electron temperature	8.8 keV
Plasma current	15 MA
Discharge duration	300-500 s
Maximum magnetic field	5.3 T
Output power	500 MW
Q	10

Table 1.1: Design parameters of the ITER tokamak.

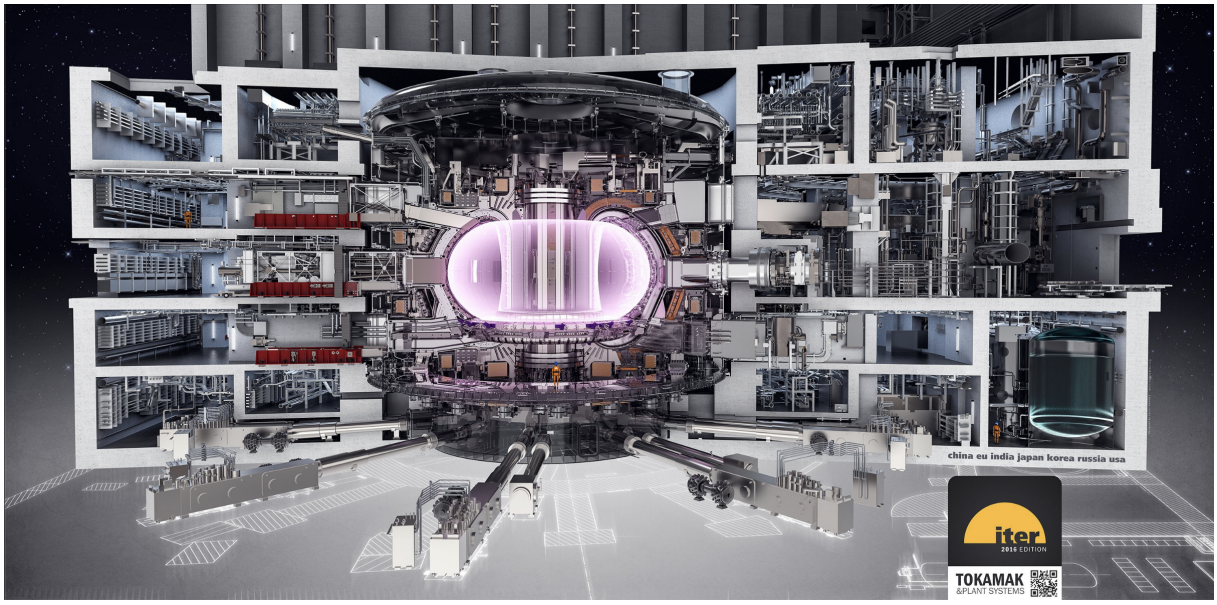

Figure 1.8: Sketch of the future ITER machine, taken from [38].

- testing technologies, in particular the tritium breeding, but also heating control, diagnostics, cryogenics, remote maintenance, divertor efficacy in eliminating the thermalized α particles;
- demonstrating the safety of a fusion device.

ITER will contribute to the design of DEMO, the *DEMOnstration Power Plant*, a project with the aim to produce electricity with a thermonuclear fusion device, not yet at a reasonable prize, but leading to the threshold of a fusion reactor prototype.

1.4 Magneto-Hydro-Dynamic Equilibrium

Being formed of free electrons and ions, a thermonuclear plasma can be considered as a quasi-neutral ionized gas, which means that the neutrality conditions (Equation 1.13) must always holds, except for local fluctuations:

$$n_e = \Sigma_i Z_i \cdot n_i \tag{1.13}$$

Charged neutrality is verified if an *ambipolar* electric field originate to oppose to a charge separation in the plasma. This field acts by accelerating the ions and de-accelerating the electrons, which indeed move faster the then former ones. Therefore, an electric potential energy, U_p, rises opposing to the thermal (kinetic) one, K:

$$\begin{cases} U_p \propto \frac{e^2 n(0)}{\epsilon_0} L^2 \\ K = k_b T \end{cases} , \tag{1.14}$$

where $n(0)$ is the plasma density at the plasma centre and L represents the plasma macroscopic length. When $U_p > K$, the plasma displays a collective behavior (*ambipolar diffusion*), which means that the motion depends not only on local conditions, but also on the state of the plasma in remote regions. When instead $U_p < K$, plasma particles show a single-particle behavior (*thermal diffusion*). When $U_p = K$, the *Debye length*

$$\lambda = \sqrt{\frac{\epsilon_0 k_b T}{e^2 n(0)}} \tag{1.15}$$

is defined and it represents the length above which the charge separation is negligible and the plasma can be considered as a single fluid.

The *Magneto-Hydro-Dynamic* (MHD) *model* is a dynamical theory that describes a fusion plasma as a magnetized fluid, under the assumption of no charge separation and non-relativistic condition (second and higher orders of $\frac{v}{c}$ are neglected). Because of the large mass difference between electrons and ions, the ions contribute mainly to the mass and the momentum of the plasma, while the electrons guarantee the quasi-neutrality condition and lead to an electrical current when their velocity is different from that of the ions. The collective (one-fluid) variables, i.e. the mass density, the current density and the centre of mass fluid velocity, are defined as

$$\begin{cases} \rho = n_i m_i + n_e m_e \sim n_i m_i \\ \mathbf{j} = e(n_i \mathbf{v}_i - n_e \mathbf{v}_e) = en(\mathbf{v}_i - \mathbf{v}_e) \\ \mathbf{v} = \frac{1}{\rho}(n_i m_i \mathbf{v}_i - n_e m_e \mathbf{v}_e) \sim \mathbf{v}_i \end{cases} \tag{1.16}$$

The *Navier-Stokes* equation, which describes the hydrodynamic equilibrium of fluids, can be then implemented with the contribution of the Lorentz force:

$$\rho \left(\frac{\partial \mathbf{v}}{\partial t} + (\mathbf{v} \cdot \nabla)\mathbf{v} \right) = \mathbf{j} \times \mathbf{B} - \nabla p + \rho \nu \nabla^2 \mathbf{v} \tag{1.17}$$

where ν and p are the plasma viscosity and pressure respectively and $\mathbf{B}$ the magnetic field. This is one of the MHD model relations, the other are the *continuity equation* (1.18), *Ohm's law* (1.19) and *Maxwell's equations* (1.20, 1.21, 1.22, 1.23):

$$\frac{\partial \rho}{\partial t} + \nabla \cdot (\rho \mathbf{v}) = 0 \tag{1.18}$$

$$\mathbf{E} + \mathbf{v} \times \mathbf{B} = \eta \mathbf{j} = \frac{\mathbf{j}}{\sigma} \tag{1.19}$$

$$\nabla \cdot \mathbf{E} = 0 \quad \text{(quasi-neutrality)} \tag{1.20}$$

$$\nabla \cdot \mathbf{B} = 0 \tag{1.21}$$

$$\nabla \times \mathbf{E} = -\frac{\partial \mathbf{B}}{\partial t} \tag{1.22}$$

$$\nabla \times \mathbf{B} = \mu_0 \mathbf{j} \tag{1.23}$$

Note that in the Ampère's law (Equation 1.23) the displacement current is neglected, which implies neglecting phenomena with phase velocity close to that of the speed of light, i.e. electromagnetic waves. $\eta = \frac{1}{\sigma}$ in Equation 1.19 stands for the resistivity of the plasma, that depends on the temperature as $\eta \propto T^{-\frac{3}{2}}$ (*Spitzer's resistivity*). This means that for very high temperatures a plasma is a very good conductor: $\eta \to 0$, $\sigma \to \infty$. If one takes this limit, Ohm's law becomes

$$\mathbf{E} + \mathbf{v} \times \mathbf{B} = 0 \tag{1.24}$$

and one obtains the *ideal MHD model*.

The MHD model is in general valid when:

- the length of the particle orbit (Larmor radius) is small compared to the macroscopic length of the system;
- the particle distribution function $f(\mathbf{x}, \mathbf{v}, t)$ in the phase space $d^3x\ d^3v$ is approximated by a Maxwellian, which implies that the timescales are long compared to the collision time.

1.4.1 MHD stability in toroidal configuration

An equilibrium state is characterized by stationarity, that is $\frac{\partial}{\partial t} = 0$. Velocity terms could be neglected, being small compared to the pressure gradient and the Lorentz force, thus Equation 1.17 reads

$$\nabla p = \mathbf{j} \times \mathbf{B} \tag{1.25}$$

which is called *force balance equation* and represents the equilibrium between the confining magnetic force and the pressure gradient that tends to bring the particles towards the plasma edges. Using Ampére's law, Equation 1.25 becomes

$$\nabla p = -\nabla \frac{B^2}{2\mu_0} + \frac{B^2}{\mu_0} \boldsymbol{\kappa} \tag{1.26}$$

where $\boldsymbol{\kappa} = \frac{\mathbf{B}}{B} \cdot \nabla \left(\frac{\mathbf{B}}{B} \right)$ is called *curvature*, since it is related to the curvature radius, $\kappa = \frac{1}{\rho_{Lar}}$. The right side shows the appearance of two kinds of restoring forces to the displacement of a field

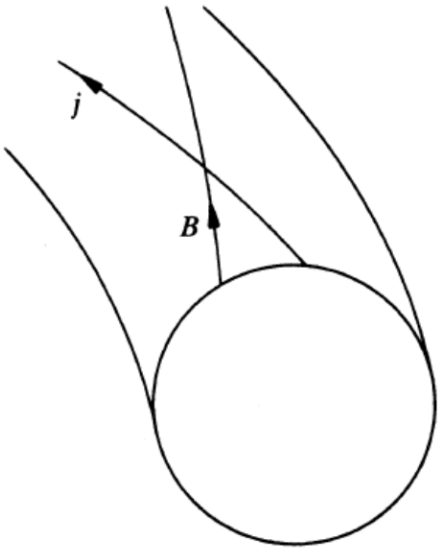

Figure 1.9: Representation of a magnetic surface hosting both the magnetic field and the current density lines.

line, that are, in order, the *magnetic pressure* and the *field line tension*. These forces give rise to two types of MHD waves, the *Compressional Alfvén Waves* and the *Shear Alfvén Waves*. The former ones are sound waves that propagates in the longitudinal direction and they are due to the magnetic pressure. The latter ones arise when the plasma is perturbed in an incompressible way and they travel along the equilibrium field lines, hence they are transverse wave. Their importance in fusion experiments will be clear in Subsection 2.5.2.

If one computes the scalar product between **B** and the two members in the force balance equation, one finds out that the pressure gradient along the magnetic field lines is zero, that is there is no variation of pressure on the magnetic surfaces. The same holds by taking the scalar product with **j**. This means that the magnetic surfaces host both the magnetic field lines and the current density lines (Figure 1.9) and they can be identified by a certain pressure value.

Furthermore, other two ingredients are required to describe the MHD stability, that are the *poloidal (magnetic field) flux function* ψ, and the *current density flux function* f. Assuming axisymmetric conditions ($\frac{\partial}{\partial \phi} = 0$), they are defined such that

$$\begin{cases} B_R = -\frac{1}{R}\frac{\partial \psi}{\partial Z} \\ B_Z = \frac{1}{R}\frac{\partial \psi}{\partial R} \end{cases} \tag{1.27}$$

and

$$\begin{cases} j_R = -\frac{1}{R}\frac{\partial f}{\partial Z} \\ j_Z = \frac{1}{R}\frac{\partial f}{\partial R} \end{cases} \tag{1.28}$$

Because $B \cdot \nabla \psi = 0$ and $j \cdot \nabla f = 0$, the magnetic surfaces are also surfaces of constant ψ and f.

By combining the MHD relations and the definitions in Equations 1.27 and 1.28, it is possible to derive the *Grad-Shafranov equation*:

$$R\frac{\partial}{\partial R}\left(\frac{1}{R}\frac{\partial \psi}{\partial R}\right) + \frac{\partial^2 \psi}{\partial Z^2} = -\mu_0 R^2 \frac{dp(\psi)}{d\psi} - \mu_0^2 f(\psi)\frac{df(\psi)}{d\psi} \tag{1.29}$$

This is a non-linear partial differential equation of the variable $\psi(R, Z)$, whose solutions represent the equilibrium states of the plasma and their constant contours give the shape of the magnetic

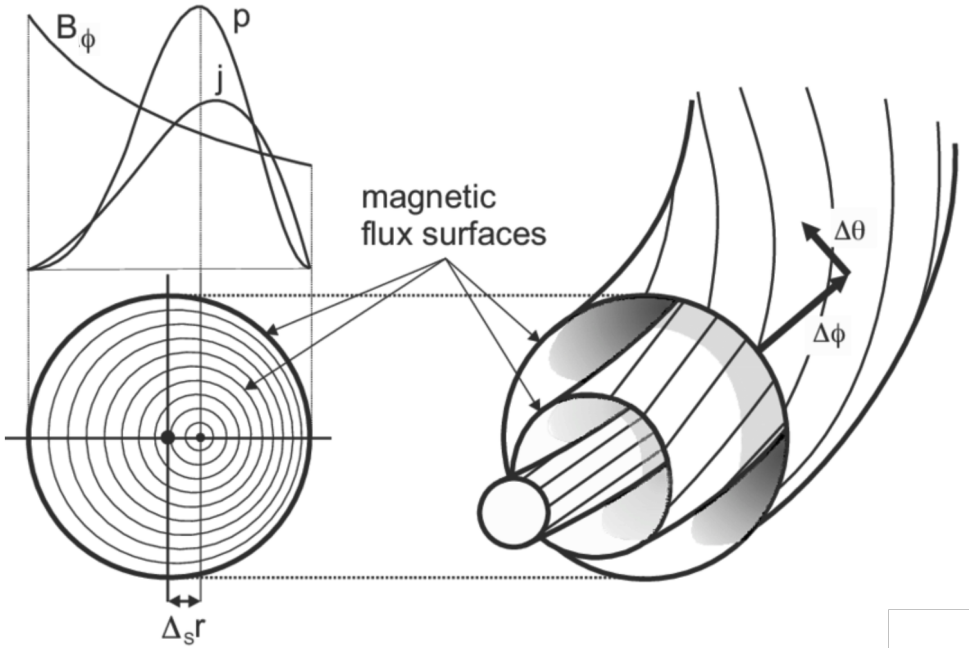

Figure 1.10: Representation of toroidal magnetic field, current density and pressure radial profiles on the poloidal cross section. Because of the non uniform poloidal magnetic field, the Shafranov shift of the magnetic surfaces centres originates.

surfaces on the poloidal plane. Figure 1.10 gives an idea of the use of Grad-Shafranov results. Because in tokamak the poloidal magnetic field is lower at the edge than in the core, the centres of the flux surfaces are shifted outwards (Shafranov shift, Δ_S).

In order to solve Equation 1.29, it is important to choose the boundary conditions, which are determined by the currents flowing in the external coils devoted to equilibrium control, plasma position and shape reconstruction, that are located in the toroidal plane externally to the vacuum vessel ("Outer poloidal field coils" in Figure 1.5). These currents allow, for example, to obtain D-shaped plasmas, through which modern tokamaks can reach higher pressure values for a given toroidal magnetic field.

1.4.2 MHD instabilities

In analogy with equilibrium states in mechanics, the solutions of the Grad-Shafranov equation can be stable or unstable, depending on the magnetic field perturbations that can develop in a fusion plasma. In the simple case of a circular plasma with a large aspect ratio ($\frac{R_0}{a} \to \infty$), any perturbation can be written as a sum of Fourier modes

$$exp\{i\,[m\theta + n\phi]\} \tag{1.30}$$

where m and n are called respectively *poloidal* and *toroidal mode numbers*, hence characterized by an helical wavefront. Perturbations that develop in a generic position in the plasma lead to a bending of the field lines, to which the restoring forces oppose, allowing to stabilize their effect. However, a perturbation can also develop at a surface in the plasma with a safety factor

$$q = \frac{\Delta\phi}{2\pi} = \frac{m}{n} \tag{1.31}$$

where m and n are the mode numbers, which is why it is called *resonant surface*. These resonant modes are characterized by the same pitch of the plasma, which means that they do not bend the magnetic field lines and no restoring effect opposes to them. This is why they are associated

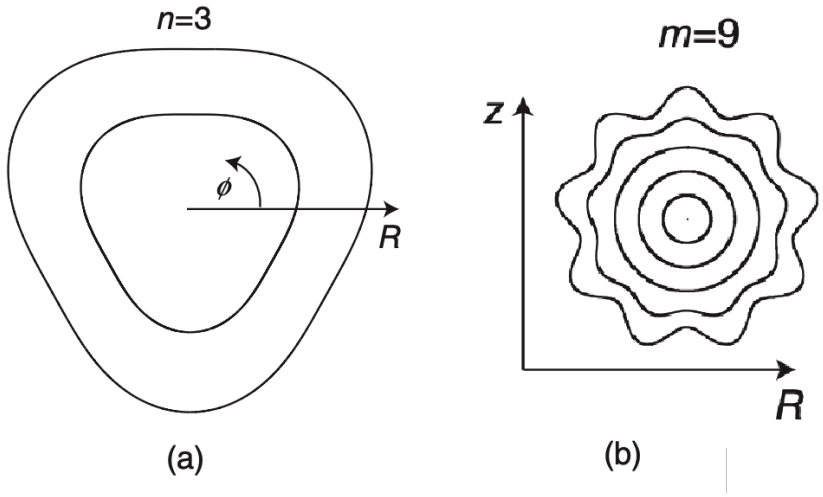

Figure 1.11: Pictorial representation of the deformations of magnetic surfaces produced by a mode perturbation with (a) n=3 and (b) m=9 mode numbers, respectively in the toroidal and in the poloidal planes.

to the most unstable situations. Figure 1.11 depicts the example of how the m=9, n=3 mode deforms the magnetic field surfaces.

Instabilities are classified basing on two criteria, that are the role of resistivity and the type of driving force.

Depending on whether it is possible to neglect the resistivity of the plasma, one distinguishes *ideal* from *resistive* instabilities.

- *Ideal instability*

  Ideal MHD stability is obtained under the assumption of infinite electrical conductivity, i.e. magnetic field lines are considered as frozen into the plasma and the motion is assumed to be flux conserving. Therefore, no change in the topology of the nested flux surfaces occurs.

- *Resistive instability*

  A finite electrical conductivity changes this picture and allows to generate or annihilate magnetic flux. The frozen-in flux constraint does not hold in this case and this makes possible a change in the magnetic surfaces topology. The characteristic timescale over which the magnetic field diffuses into a plasma of cross section L^2 is the *resistive time*

  $$\tau_R = \mu_o \sigma L^2 \tag{1.32}$$

  Hence for $t \ll \tau_R$ the flux is conserved and ideal MHD is valid.

In general, if a plasma is ideally unstable it will be unstable also if finite resistivity is taken into account, while finite resistivity is associated to perturbations that would not be possible in the ideal case. Ideal modes are the most violent: because they do not have to change the magnetic topology, they grow very fast and lead to premature discharge termination, to which one refers as *disruptions*. Resistive modes have a negative effects on plasma confinement, that can in turn initiates a disruption too.

The second classification discriminates between *pressure-driven* and *current-driven* instabilities.

- *Pressure-driven instability*

  This kind of perturbations are related to the interplay between the pressure gradient and the curvature of the magnetic lines. The pressure gradient is perpendicular to the magnetic

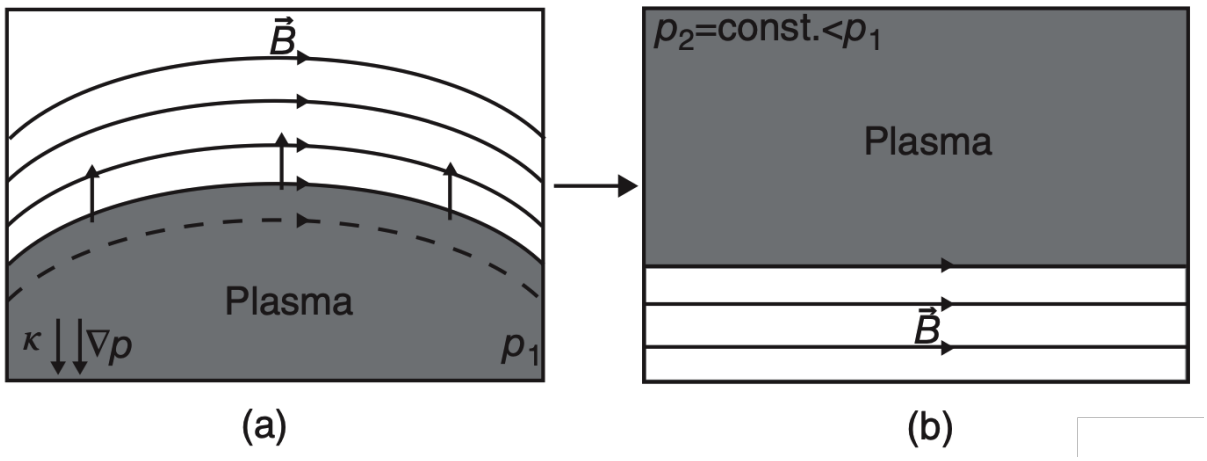

Figure 1.12: Sketch of the principle that governs the pressure-driven perturbations: depending on their curvature with respect to the pressure gradient, the field lines are shortened (a) or lengthened (b) when interchanged with the plasma. In the first case the equilibrium is unstable, in the second one is stable.

flux, hence it has the same direction of the curvature vector $\boldsymbol{\kappa}$. If the two vectors are parallel the effect of these perturbations is destabilizing, whereas if they are anti-parallel it is stabilizing. These two situations have been called 'bad' and 'good' curvatures respectively. Figure 1.12 depicts an intuitive sketch of the phenomenon that occurs, assuming that there is a region filled with plasma surrounded by a region of magnetic field that confines it. Panel (a) represents the "bad" curvature case, in which, if one imagines to interchange the plasma and the magnetic field, the magnetic field lines will shorten as the plasma expands, thus lowering the energy of the system. In panel (b) the opposite happens, since the "good" curvature leads to the lengthening of the field lines and hence an increase of the plasma energy during the interchange. In toroidal systems, the core of the torus is a region of good curvature, while the edge has a bad curvature, therefore the result is an expansion of the plasma in the outer region, that resembles a balloon. This is why these instabilities are usually called *ballooning modes*.

- *Current-driven instability*

  These perturbations are driven by the current density parallel to the magnetic field, hence the curvature of the toroidal field is not that important in this case. Magnetic surfaces kinks belong to this class of instabilities, which cause the bending of the plasma column (Figure 1.13). The unstable kink perturbations are incompressible, they drive a torque $T_{kink} = \mathbf{B}(\nabla \cdot \mathbf{j})$ and therefore their destabilizing effect is linked to the current density gradient, $\frac{dj_\phi}{dr}$.

Instabilities in real systems are usually a mixture of all these types.

1.4.3 Tearing modes

As explained previously, the assumption of perfect conductivity implies the fixed topology of the magnetic field, but this is an unreal constraint that leads to an overestimation of the plasma stability. The finite resistivity introduces new modes that play a role mostly in a narrow layer around their resonant surfaces, at which the magnetic field lines break and then re-join. This is why one refers to these resistive perturbations as *tearing modes* (TM). They are current-driven instabilities, since they are due to a strong gradient in the current density profile parallel to the magnetic field ("classical" tearing modes). While tearing modes with $m > 3$ can be easily stabilized by tailoring properly the plasma current, the most unstable modes are the ones that develop at low-q resonant surfaces (Figure 1.14).

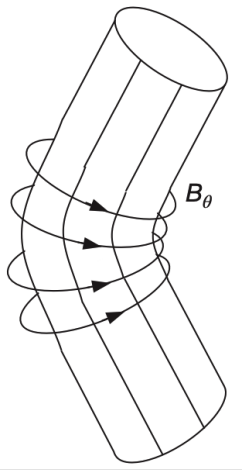

Figure 1.13: Bending of the plasma column caused by a kink instability.

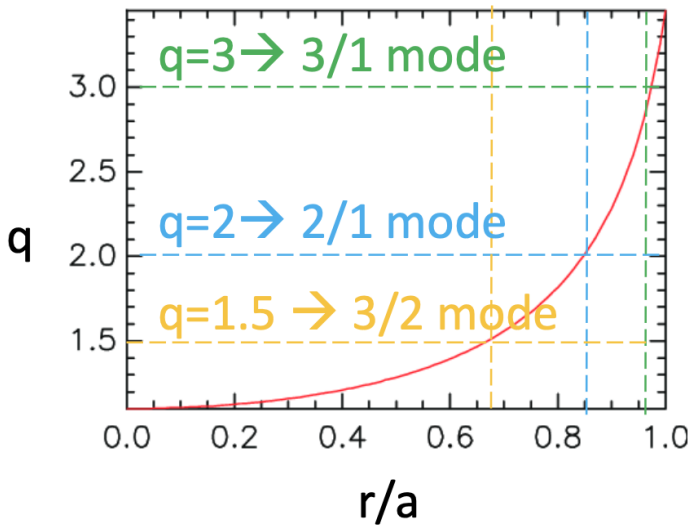

Figure 1.14: Typical safety factor of a tokamak as a function of the radial coordinate normalized to the torus minor radius. The resonant surfaces associated to the most destabilizing tearing modes are underlined.

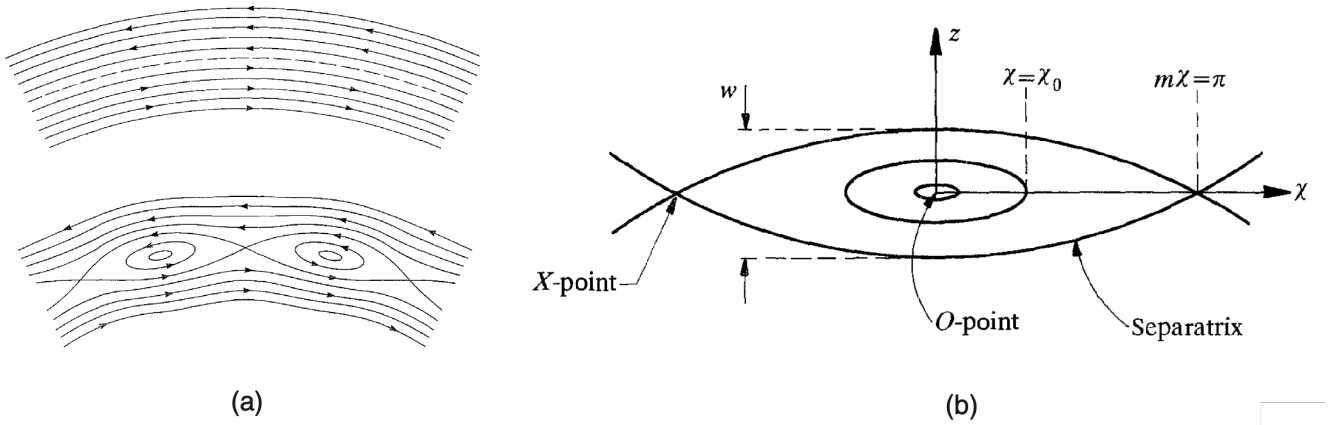

Figure 1.15: Sketch of (a) the reconnection of opposite directed field lines in the current sheet and of (b) the main magnetic island characteristics.

The process through which magnetic field lines re-join after the tearing is called *reconnection* and it happens in a region called *current sheet*, where a steep current gradient causes the frozen flux constraint not to hold. Here, magnetic field lines in opposite directions can be found very close to each other, which makes possible their reconnection in the so-called *magnetic islands*, which thus appear as regions in the plasma with a different magnetic topology. In Figure 1.15 a pictorial representation of the reconnection (panel (a)) and of a typical magnetic island (panel (b)) are shown.

It is possible to demonstrate theoretically [34] that the tearing mode instability is mainly due to the *bootstrap current*, a self-generated current in the plasma, that originates from the collisions between trapped and passing particles. In fact, because the poloidal current generated by the trapped particles motion is unbalanced since the density is not constant, the bootstrap current is needed to "close the circuit". Let us consider an initial perturbation associated to a small island on a rational surface. The unstable behaviour is due to the flattening of the kinetic (temperature, pressure) profiles in the island, that will be explained in Subsection 1.4.4. The pressure profile flattening causes the bootstrap current density to reduced, creating a hole in its profile at the resonant surface, which in turn increases the width of the island, that further enhances the pressure flattening. This unstable situation is the basic mechanism of the *neoclassical tearing modes* (NTMs). They can be regarded as pressure-driven resistive instabilities, since they are related to finite pressure gradient at the resonant surface.

1.4.4 Intrinsic error field and locked modes

Another type of magnetic perturbation is the intrinsic Error Field (EF), which is due to non-axisymmetric inaccuracies in the manufacturing and the assembly of magnets, joints, feed lines, ferromagnetic materials near the plasma surface. An EF is inevitably present in fusion devices and interacts with the plasma through by multiple mechanisms, such as rotation braking, confinement degradation, energy and particle loss, MHD activity onset, potentially causing a disruption. Such kind of dynamics can not be tolerated in future disruption-adverse tokamaks, such as ITER. In particular, focusing on what concerns this thesis, the presence of the machine intrinsic error field is related to the locking mechanism of tearing modes.

A TM can induce eddy currents in the vacuum vessel, which can in turn create a drag force on the mode that acts by decreasing its phase velocity. When it is reduced to zero, the mode is locked to the vessel. In general, there is always a small driving effect that opposes the complete locking, tending to restore the natural frequency of the mode. However, if an intrinsic error field is present in the machine, it can drive an electrodynamic torque that locks completely the island

to the EF frame. This has been confirmed by the evidence that, in many tokamaks, it has been found that the position of a locked mode of a given helicity is always the same with respect to the vacuum vessel, indicating that the breaking of the axisymmetry of the magnetic field plays is crucial.

Furthermore, from both empirical evidences and theoretical arguments, it is known that, when the amplitude of the external perturbation, responsible for the tearing mode onset, is above a certain threshold, the linear reconnection of the field lines bifurcates, leading to a sharp increase of the island width. At this point a non-linearly amplified regime is established, in which the locking mechanism happens. This process is known as *error field penetration*. The island starts to grow in size until along its whole width the pressure profile flattens and heat and particles fluxes towards the walls occur, leading to the reduction of the stored energy in the plasma, which can cause a disruption. In fact, the transport coefficient in a hot magnetized plasma is in general low in the direction perpendicular to the magnetic field lines, thus magnetic islands represent a sort of shortcut for radial heat and particle fluxes.

It is worth mentioning that also *ab-initio* locked modes have been observed, i.e. magnetic islands grown in a locked state from the beginning, indicating that the error field has played a role already in their generation. This is often observed in low plasma density regimes, as documented in [4], [64].

1.5 Thesis Objectives

The presence of a locked mode affects plasma rotation. In particular, at JET the braking effect covers a large fraction of the rotation profile, while a spin up of plasma rotation has been observed at the edge, in particular at the $q = 2$ surface.

This is a matter of concern for plasma operation, because when this occurs MHD instabilities can be triggered and turbulence level increases [65]. In particular, this study is crucial for ITER operations, where the plasma rotation is foreseen to be small, thus efforts to find new evidences and review the obtained results must be made, collecting data in present magnetic fusion devices which are gathered in Ohmic regimes.

In this context, this Thesis project aims to understand how plasma rotation and magnetic island triggering are related and how a change in one the two affects the other, considering the most recent experiments performed at JET in Ohmic regimes.

The objectives for this work are the following:

- characterization of the plasma rotation in presence of externally induced locked modes;
- assessment of the role of neutral beam injection in spinning up the plasma rotation, hence avoiding the locked mode onset.

Chapter 2

The Joint European Torus

In this chapter, the Joint European Torus device is briefly described, with a focus on its main systems and diagnostics that are involved in this Thesis work: the Neutral Beam Injection system, the Error Field Correction Coils, the Mirnov coils array and the Charge Exchange Recombination Spectroscopy.

2.1 JET Overview

The Joint European Torus (JET) is the largest tokamak device of approximately 15 metres in diameter and 12 metres high, with a total plasma volume of 90 m^3. It was the first experiments that used a 50-50 mix of tritium and deuterium in 1991. In 1997, JET set a world record for fusion output, producing 16 MW from an input of 24 MW of heating, reaching the record Q value of 0.67, for a short instant of time ($\sim$1 second). In 2021 a new world record of 59 MJ was achieved in JET in a 5 s pulse, while burning only 170 μg of deuterium and tritium. In October 2023, 69 MJ with 0.2 mg of fuel in a 5 s pulse set the ultimate world record regarding the output power, but not for the gain parameter ($Q = 0.33$).

The core of the machine is the toroidal vacuum vessel, characterized by a D-shaped cross section, whose dimensions are reported in Table 2.1, together with the other main design parameters. The toroidal magnetic field is generated by thirty-two D-shaped coils equally spaced around the torus, made of copper windings. The poloidal magnetic field is instead generated by inner coils (primary windings) located in the centre of the machine, that are coupled with the plasma (secondary circuit) by the massive eight limbs of the iron transformer. Outside the machine, but still within the transformer limbs, a set of six field coils is used for plasma position and shape control. Being made of a conductive and not a superconductive material, JET coils need to be water-cooled after their usage. In 2011 the ILW were installed, replacing the carbon walls. The described device is depicted in Figure 2.1 and 2.2.

Parameters	**Values**
Major radius	2.96 m
D-shape cross section	2.5 m $\times$ 4.2 m
Electron temperature	10 keV
Plasma current	5 MA
Maximum discharge duration	1 s
Toroidal magnetic field	3.45 T

Table 2.1: Design parameters of the JET device.

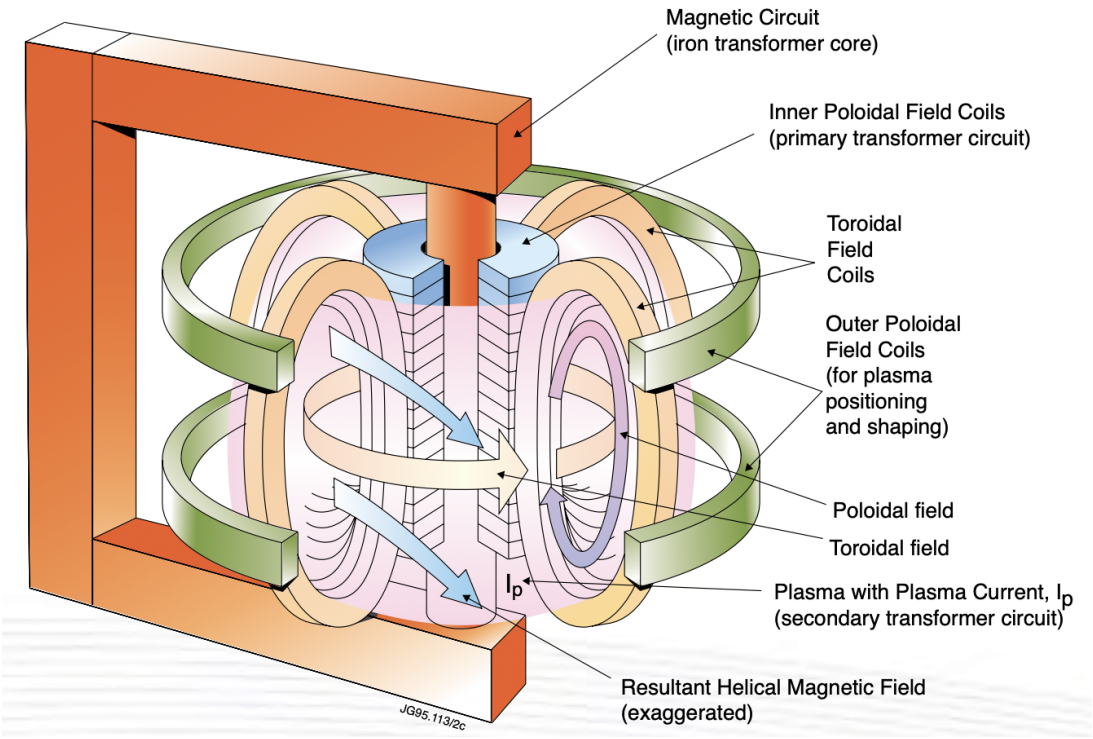

Figure 2.1: Sketch of the JET device, depicting one transformer limb, the sets of coils that generate the magnetic field and the position and shape control coils.

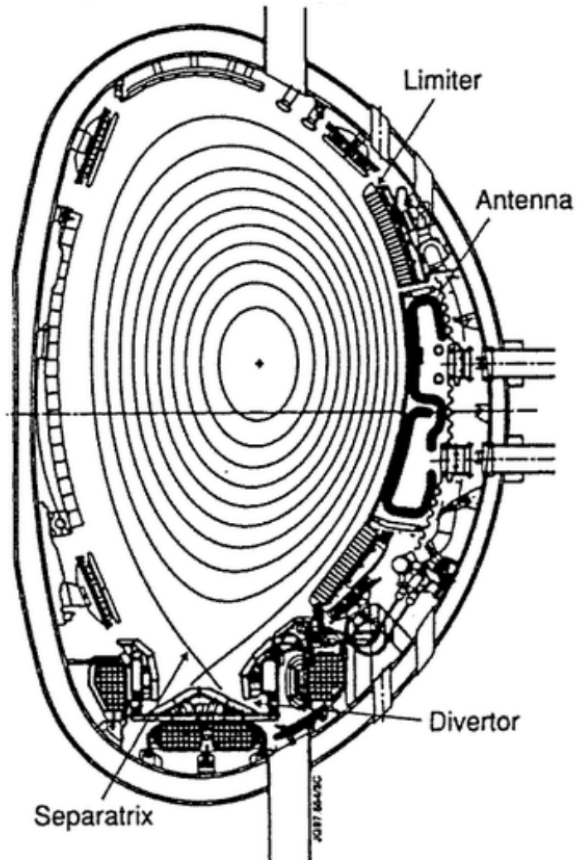

Figure 2.2: Poloidal cross section of the JET machine, showing the characteristic D-shape and the nested magnetic field lines.

JET operates in a pulsed mode, with at a maximum rate of about one pulse every twenty minutes and each pulse can last up to 60 s, even thought the usual duration is some tens of seconds. Temperatures of the order of 10^8 K are achieved and sustained thanks to the powerful heating: 34 MW from the Neutral Beams Injection (NBI), 10 MW from the Ion Cyclotron Resonance Heating (ICRH) and few MW from Ohmic heating. The energy confinement time is close to 1 s, hence, considering a power consumption well above 10 MW, the total thermal energy of a typical JET plasma is more than 10 MJ.

2.2 External Heating Systems

In contrast to metals, at millions of degrees and above a plasma is characterized by a very little resistance, which means that the heating power produced by the Joule Effect is also low:

$$\begin{cases} \eta \propto T^{-\frac{3}{2}} \\ p_{Ohm} = \eta j^2 \end{cases}$$

where η is the Spitzer's resistivity, j is the plasma current density and p_{Ohm} the power per unit of volume produced by the Joule Effect. Additional heating sources are thus required to make the fusion reactions happen. In present tokamaks, neutral particles and resonant electromagnetic waves are exploited to achieve this purpose. Moreover, these technique can drive an additional current in the plasma, that is appreciated since no transformer can provide continuous direct electric current in its secondary circuit, preventing in this way the tokamak to maintain a continuous electrical current in the plasma. This is a matter of concern if one would like to confine the plasma continuously.

2.2.1 Neutral beam injection

When neutral atoms are sent into the plasma, they loose electrons through collisions with plasma particles, becoming ions subject to the magnetic confinement. These new ions are much faster than the average plasma particles. Through further ion-ion, ion-electron, electron-electron collisions, the kinetic energy of the injected particles is transferred to plasma particles, causing an increase of their chaotic motion that means an increase in their temperature. In particular, the energy of the neutral particles is chosen so that it will be deposited near the plasma core and is usually of the order of hundreds of keV or more. This external heating system is called *Neutral Beam Injection* (NBI). The first step to generate a neutral beam is to produce large amounts of ions of the desired specie, then to accelerate them in a strong high-voltage electric field and finally to neutralise them, exploiting the charge exchange[1] interaction with a neutral gas cloud (*neutralizer*). Residual fast ions are deflected by an electromagnet to a cooled ion dump, that can withstand a heavy ion bombardment. A vacuum pumping is utilized to assure that no slow atoms from the gas cloud diffuse into the plasma chamber. Figure 2.3 show a sketch of the described procedure.

In fusion experiments, the neutral beams are usually of the same species of the plasma ions. At JET, hydrogen, deuterium and tritium injection is indeed possible. The JET NBI system consists of two Neutral Injector Boxes (NIBs) equipped each with eight Positive Ion Neutral Injectors (PINIs). They are placed in octant 4 and 8, as shown in Figure 2.4, and they can provide both tangential and normal injection. The normal injection is associated with losses due to the ripples of the magnetic field and to the possibility that a fraction of the beam crosses the plasma without interacting, hence hitting the back wall. The tangential injection is usually chosen, since it is characterized by a lower damage risk and it can be beneficial for stabilizing both turbolence and MHD instabilities. This possibility will be investigated in Section 3.4. A 3-D scheme of JET NBI system is presented in Figure 2.5 a, together with an elevation view in panel (b).

[1] Section 2.6

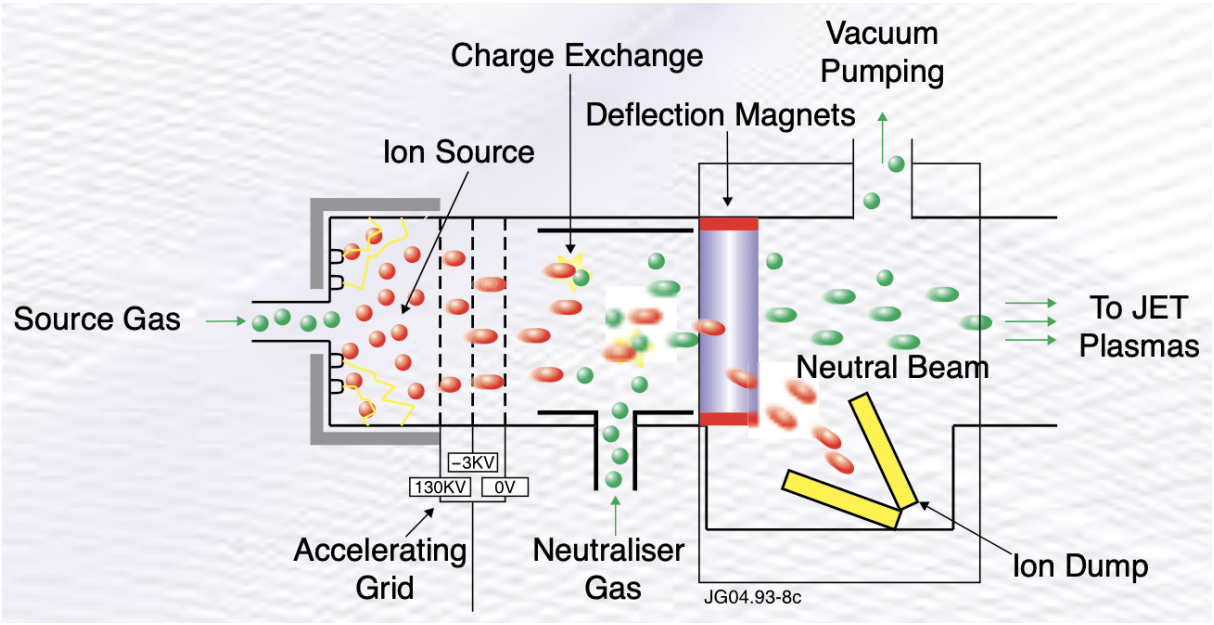

Figure 2.3: Sketch of the neutral beam production. Ions are depicted in red, neutral atoms in green.

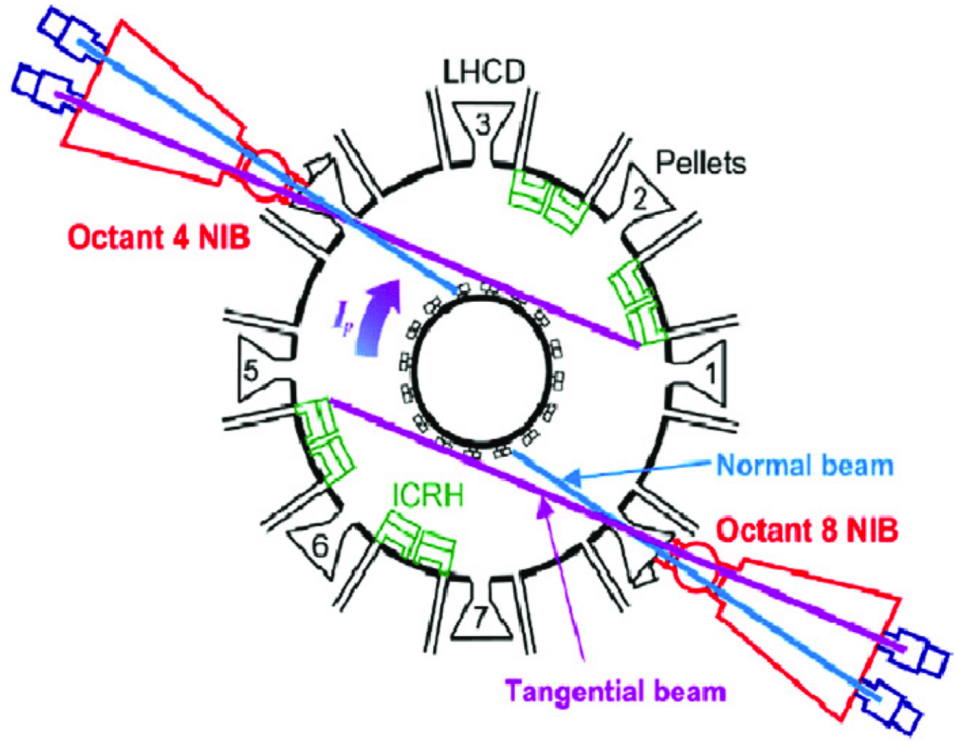

Figure 2.4: JET toroidal view, showing the main injectors sites.

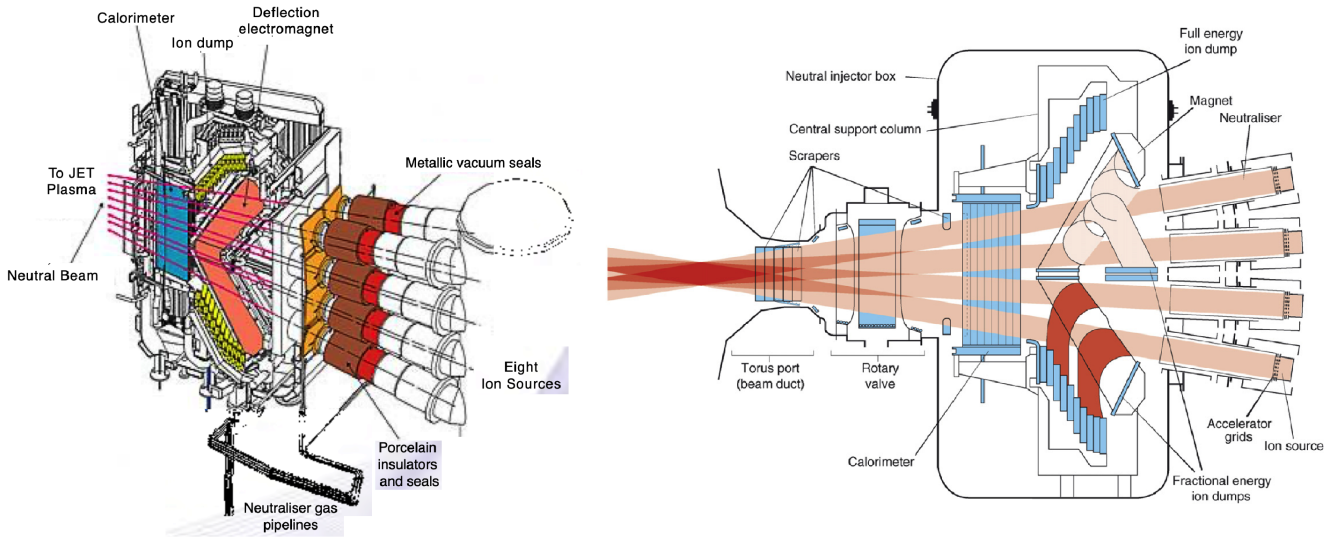

Figure 2.5: (a) Scheme of one of two identical NBI systems at JET. (b) Elevation view of one of the two JET NBIs.

JET PINIs are connected to a high voltage power supply of 130 kV/130 A. The system can provide a maximum injected power of 34 MW (deuterium neutral beam) for pulses that can last up to 20 s (40 s for half maximum power).

2.2.2 Electromagnetic waves heating

For the sake of completeness, also the other heating technique is briefly presented, even though it has not been used during the data acquisition of interest for this Thesis.

Being formed by charged particles, a plasma is affected by long-range electric and magnetic forces, therefore it hosts a variety of oscillations: mechanical, electrostatic, magnetic and electromagnetic waves. Depending on the local plasma parameters, plasma waves can propagate, get absorbed, be reflected or converted into a different type. In general, plasma waves carry energy, hence their absorption involves an energy transfer to the plasma particles, which increases their chaotic motion and thus their temperature. This is why sending electromagnetic waves into the plasma is an heating process. The probability of absorption of an external wave increases when its frequency matches an intrinsic frequency of the plasma, that is when a resonance occurs. In magnetically confined plasmas, charged particles rotate around the magnetic field lines with a cyclotron frequency

$$\omega = \frac{qB}{m}, \tag{2.1}$$

where q and m are the charge and the mass of the particle respectively and B is the magnetic field. Therefore, if an electromagnetic wave with the cyclotron resonant frequency of the ions/electrons is launched into the plasma, all the ions/electrons are heated. In tokamaks, the magnetic field decreases with the distance from the major axis, hence also the cyclotron frequency follows this trend. By changing properly the external wave frequency, it is thus possible to heat specific vertical layers within the plasma.

Ion Cyclotron Resonance Heating

The *Ion Cyclotron Resonant heating* (ICRH) exploits electromagnetic waves with a frequency resonant with the ions, i.e. Radio-frequencies (RF). At JET, RF are chosen to be resonant with the second harmonic frequency of the main JET plasma ions (deuterium) or with the base

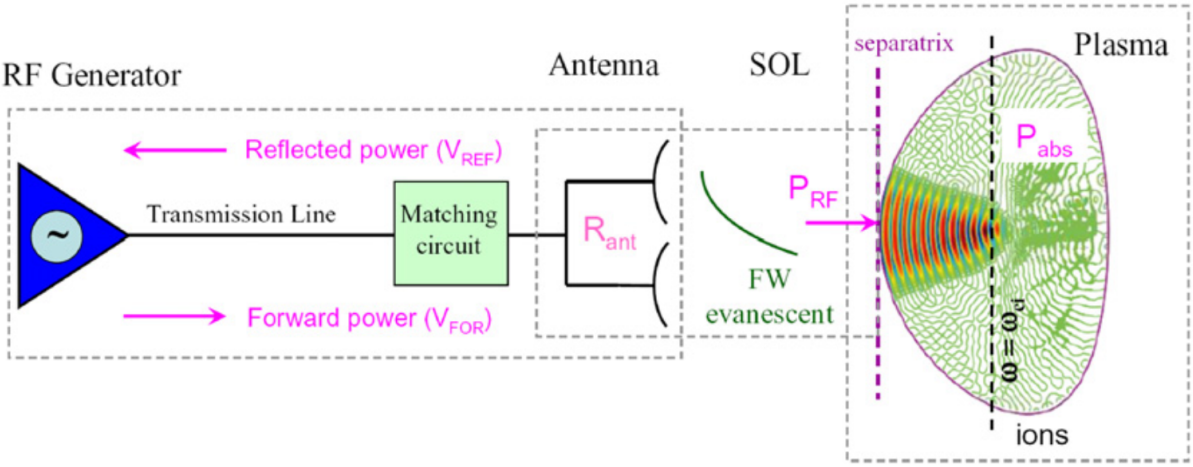

Figure 2.6: Principle of an ICRH system.

frequency of the minority species (e.g. tritium). In particular, the available resonant frequencies are in the range 23-57 MHz. In total, the installed power of JET ICRH system is 32 MW, but in practice only 10 MW are enough for JET experiments.

JET ICRH system starts with amplifier chains that generate the electromagnetic waves, each of them providing an output power of 2 MW. ICR waves are sent from the generators to the tokamak through transmission lines, that are low loss coaxial cables. They look like pipelines with 20 cm diameter and several hundreds meters of them are installed at JET. The transmission lines terminate with four ICRH antennas, installed within the JET inner walls, each of them consisting in four conductive straps, that are fed separately with four generators. The ICR waves cannot propagate in the JET vacuum vessel, since their wavelength is too long, this is why the antennas are placed as close as possible to the plasma (see Figure 2.4). Figure 2.6 shows the working principle of a typical ICRH apparatus, while Figure 2.7 depicts a scheme of the system installed at JET.

Electron Cyclotron Resonance Heating

When the wave frequency is chosen in order to heat plasma electrons, the *Electron Cyclotron Resonant Heating* (ECRH) is exploited. Being electrons several thousand of times lighter than ions, their cyclotron frequencies are higher (Equation 2.1), therefore in tokamak plasmas the required ECR frequencies are of the order of 100 GHz. It is more challenging for the generator and for the transmission lines to handle with such frequencies; moreover, ECRH targets plasma electrons only and the heat transferred from electrons to ions is relatively low. JET is indeed not equipped with an ECRH system. However, the advantage of ECR waves is that they can propagate in vacuum.

Lower Hybrid Current Drive

In a tokamak plasma other resonant frequencies can be found, but experiments have showed that their usage is either inefficient or impractical or waves at that frequencies can not penetrate through the plasma edge. An interesting case is represented by the so called *hybrid frequencies*, which lie between ion and electron cyclotron spectra. They can propagate into the plasma, but their heating effect is inefficient. Nevertheless, they are able to drive an electric current and this is why JET is implemented with a Lower Hybrid Current Drive system, which generated waves with frequency of 3.7 GHz by means of twenty-four klystrons. They travel through waveguides until they reach an antenna mounted directly on the inner wall, as close as possible to the plasma.

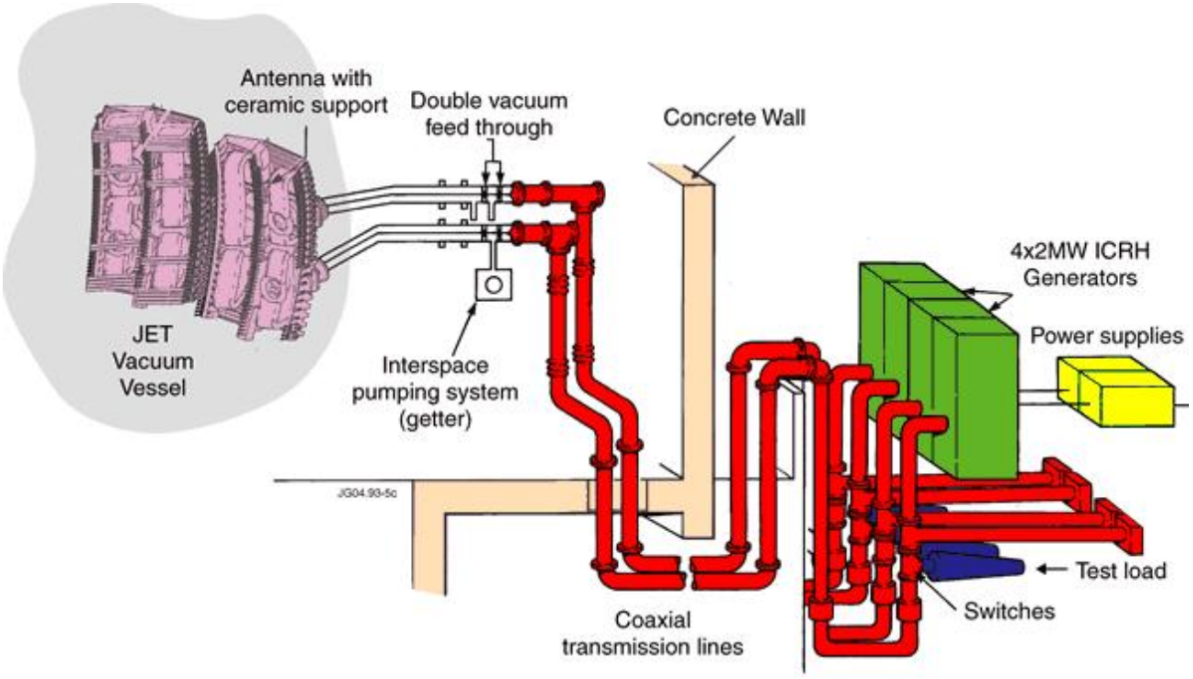

Figure 2.7: Scheme of the ICRH system at JET.

Nominally its heating power is 12 MW, which corresponds to an electric current of several MA. The described system is schematized in Figure 2.8 and its location can be seen in Figure 2.4.

2.3 Error Field Correction Coils

Outside the vacuum vessel, JET is also provided with a set of four Error Field Correction Coils (EFCCs), that are located in the four octants, 1,3,5,7. Each coil spans 70° in the toroidal direction and is placed at a radial distance from the axis of the torus from 5.3 to 7 m. They are made of 16 turns, carrying a maximum current of 6 kA. Figure 2.9 and 2.10 show respectively the perspective and the toroidal view of the system.

The EFCCs were first installed at JET to perform error field identification experiments, by inducing a controlled perturbation with these coils set. This method will be explained in details in Section 3.1. In particular, at JET [21] it has been documented that most of the natural disruption events are due to the presence of a n=1 locked mode, that is why several investigations on this instability have been carried out by exploiting the EFCCs system. It can be wired both in a n=1 and a n=2 locked mode configurations. The n=1 configuration, in particular, is created by feeding opposite EFCCs (180° toroidally apart) with oppositely directed currents. Moreover, by varying the EFCC current polarities in the quadrature pairs of coils, the toroidal phases of the induced magnetic field perturbation can be varied.

EF identification is not the only type of experiments that exploited the EFCCs at JET. In the following, other examples are briefly presented, all of them setting the EFCCs in the n=1 or n=2 configuration.

- *Probing plasma stability above the no-wall β-limit*

  In order to provide safe steady-state operation of future reactors, ensuring plasma stability at high plasma pressure is a fundamental requirement, that is mainly threatened by the Resistive Wall Modes (RWMs), a class of kink-like non-axisymmetric instabilities, in advance tokamak scenarios. A safe way of probing no-wall stability consists in examining the plasma

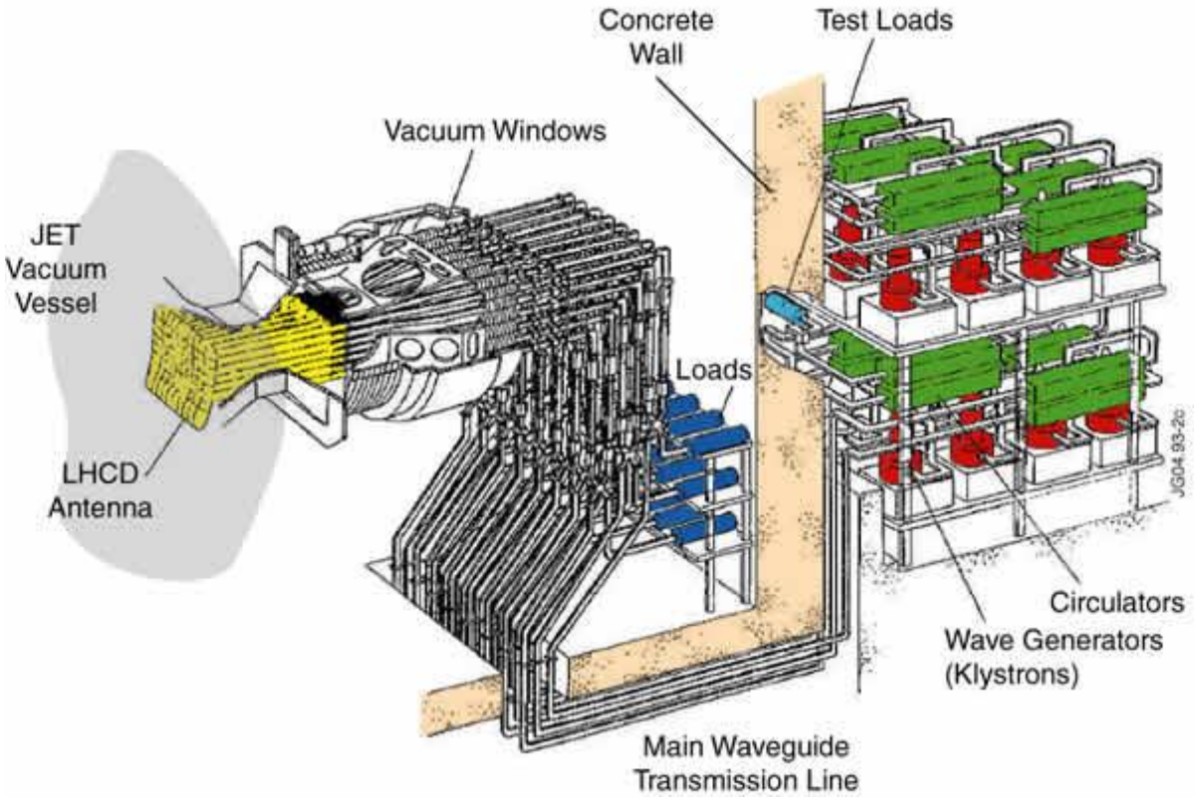

Figure 2.8: Scheme of the LHCD system at JET.

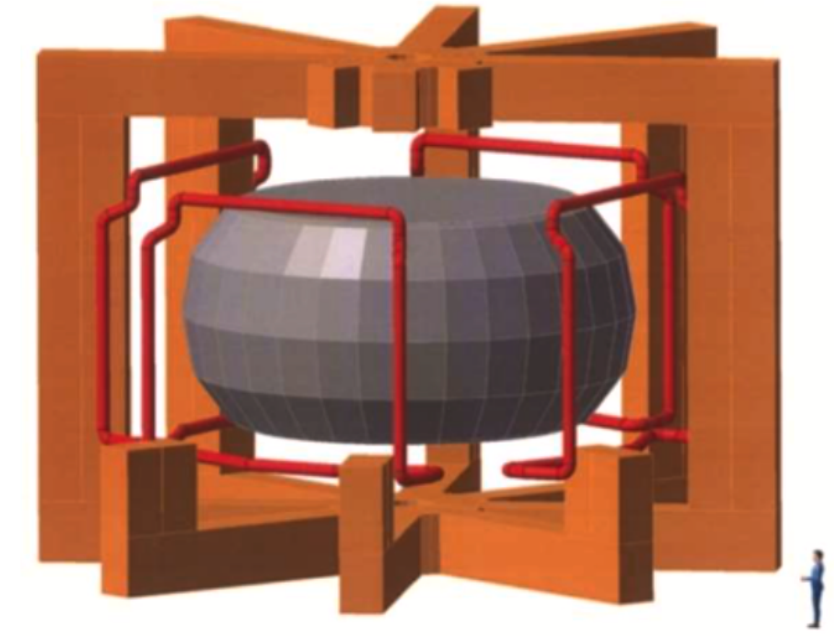

Figure 2.9: Perspective 3-D view of the EFCCs system at JET.

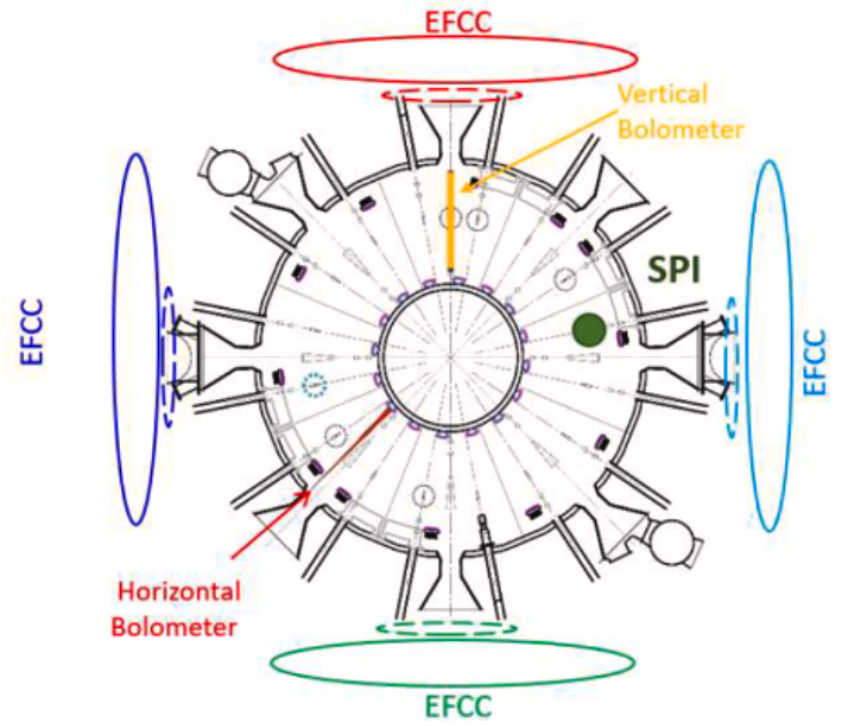

Figure 2.10: Toroidal view of the JET machine, showing the EFCCs (solid lines), the saddle loop sensors (dashed lines), the horizontal and vertical bolometers and the location of the pellet injection (SPI).

response to externally applied magnetic fields, in particular with n=1 perturbations. In fact, at JET [46] it has been observed an enhancement of the plasma response to the external perturbation when $\beta_N > \beta_N^{no-wall}$, where

$$\beta_N = \beta \frac{B_t(T)a(m)}{I_p(MA)} \propto p \tag{2.2}$$

is the normalized β-parameter, related to the toroidal magnetic field B_t, the plasma current I_p and proportional to the plasma pressure p. The no-wall normalized β-parameter, $\beta_N^{no-wall}$, is calculated in the ideal condition of absence of walls.

- *Radiation asymmetry investigation during mitigated disruption*

  The Disruption Mitigation System (DMS) of JET is equipped with a Shattered Pellet Injection (SPI) that injects impurities in the form of frozen shattered material with a guide tube, in order to dissipate a fraction of the plasma thermal and magnetic energy through the emission of radiation, thus mitigating the thermal load to the first wall and to the divertor and largely avoiding runaway electrons. Because pellet spatial distribution is not uniform in the plasma, it is required to avoid strong radiation asymmetries, to prevent local melting of the first walls associated to radiation power peaks. As anticipated, n=1 locked mode usually triggers natural disruptions at JET, hence studies [43,44] on radiation distribution in presence of this perturbation have been carried out, by inducing this type of mode through the EFCCs. Two bolometers (see Figure 2.4) have been used to measure the radiation power of different types of pellet, with different sizes and velocities.

- *Control of edge localized mode*

Edge Localized Modes (ELMs) are MHD quasi-periodic instabilities which originate as an intrinsic feature of the high confinement regime, because of the steep pressure profile at the plasma edge. As magnetic perturbations, ELMs are potentially dangerous since they cause heat and particle flux to the first walls, but they could also provide a means to flush impurities from the plasma, if their frequency and amplitude are properly controlled. In particular, external magnetic field perturbations can be used to mitigate or suppress ELMs: at JET [45] this has been successfully obtained by inducing n=1 and n=2 modes through the EFCC system.

Because the magnetic field perturbation is applied externally to the machine, it has been investigated whether different wall materials would affect differently the error field penetration. The results of this study are reported in [1]. By varying the frequency of the EFCCs currents between 0 and 100 Hz, experimental data of the radial magnetic field amplitude and phase in the ILW case have been observed to matched the data collected for carbon walls, thus ensuring that the error field penetration is not sensitive to the type of wall material.

2.4 Magnetic Diagnostics

Magnetic diagnostics are fundamental to characterize a fusion plasma, since they provide information about the plasma current, the toroidal and poloidal magnetic fields, the plasma shape and position, the loop voltage, the q-profile, the magnetic instabilities and much more. These diagnostics rely on the physical principle of electromagnetic induction, being based on coils whose surface is across by a time-variable magnetic field, which thus induces a current in them, that is then collected by a passive circuit. In particular, nowadays arrays of coils, called Mirnov coils, are placed both inside and outside the vacuum vessel.

JET tokamak is equipped with hundreds of magnetic sensors distributed all over the torus, designed to withstand the neutron fluence. Fast magnetic Mirnov coils are exploited to study MHD instabilities, while slow coils are used for equilibrium reconstruction. By the end of 2016 experimental campaign, JET lost several pick-up coils. In the previous design, slow coils were based on a Mineral Insulated Cable wound around a stainless-steel, while the Mirnov coils were based on a non-insulated cable wound around a ceramic alumina former. 27 faulty in-vessel coils were refurbished [23], replaced with new fast sensors made of a Glidcop wire wound around a ceramic former, handleable with remote control.

JET magnetic diagnostic is also provided with ex-vessel Hall probes, located near to the transformer to investigate the magnetic field in the Iron limbs.

In this thesis project, the magnetic diagnostics of interest are the Mirnov coils for MHD investigation and the saddle loops for the measurements of the locked mode amplitude. Their combined usage in the locked mode detection will be explained in Section 2.5.

2.4.1 Saddle coils role in the Real-Time Control System

Eight sets of eighteen independent loops are present and placed in the external frame of the eight octants, covering the whole poloidal external surface of the torus. They are classified as:

- upper pick-up coils, for the detection of the tangential and normal field in the upper in-vessel region;
- outer pick-up coils, for the detection of the tangential and normal field in the outboard in-vessel region;
- divertor pick-up coils, for the detection of the vertical and horizontal field in the lower in vessel region.

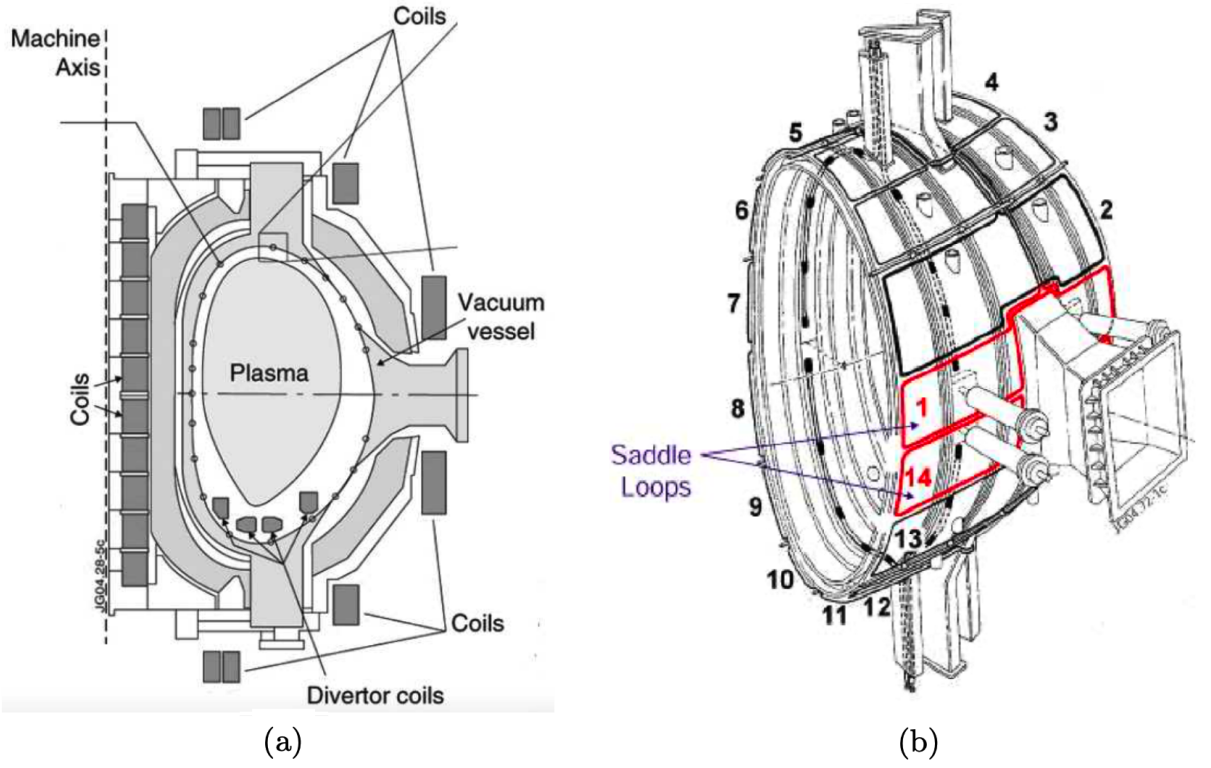

Figure 2.11: Poloidal cross section of JET torus, showing (a) all the 18 coils set and (b) the coverage of fourteen poloidal coils devoted to MHD activity studies in a specific octant. The saddle coils are the ones closest to the midplane (1 and 14 poloidal positions).

A representation of them in a specific octant is shown in Figure 2.11: in panel (b), the saddle coils are highlighted, that are the ones closest to the midplane, i.e. the 1 and 14 poloidal positions. A subset of these 8×18 coils is used for the real-time plasma shape control, while the saddle coils are devoted to the calculation of the normalized locked mode amplitude, that is one of the metrics in the JET real-time protection system. In particular, it is computed as the ratio between the linear combination of the radial magnetic field measurements, provided by the 1 and 14 poloidal position coils, and the plasma current. When the normalized locked mode amplitude overcomes the 0.2 mT/MA threshold, JET Real-Time Central Control (RTCC) triggers the Disruption Mitigation Valve (DMV). The valve is located on the top of the torus and it injects gas into the plasma when it is activated. As a result of the interaction between the injected gas and the plasma, the plasma energy is in part dissipated by the emission of radiation, so that damages to the machine components are avoided.

In general, a real-time control system consists in sensors, that measure the changes of some parameters over the time, and actuators, which alter in some way the plasma conditions. For example, at JET magnetic coils, gas valves, NBI, pellet injectors, ICRH can act as actuators. The real-time control allows instantaneous modification of the actions of the actuators, according to a comparison between the predicted plasma parameters and the sensors signals, that is made possible thanks to both a process model based on plasma physics equations and real-time measurements. JET for example makes real-time measurements of neutrons flux, magnetic flux, plasma temperature, density, helicity, X-ray, UV, visible and IR radiation, so that a real-time analysis can be made on magnetic fields, confinement, spectral lines, chemical composition, profiles of temperature, density and current. In this way a large variety of plasma scenarios can be tuned and stabilised, the maximum performance are achieved and specific experiments are carried out.

2.5 Detection of Locked Modes at JET

A locked mode detector aims to identify a non-rotating and non-axisymmetric magnetic field perturbations associated with the onset of a locked mode. At JET, a novel locked mode detector proposed in [7] has been recently designed and included, which operates by calculating the locked mode amplitude and seeking for signatures of the Beta-induced Alfvén Eigenmodes (BAEs).

2.5.1 Saddle coils role in locked modes detection

The saddle coil sets are exploited during EF identification studies to look for evidences of locked mode onset, by calculating the time variation of the external radial magnetic field amplitude. In contrast with the RTCC working principle, the normalized amplitude of the locked mode induced by the EFCC ramp is not a good metric in this case, since the saddle loops signal is affected by the magnetic pick-up introduced by the EFCCs.

A compensated radial magnetic field represents thus the exploited metric, which is calculated by subtracting the n=1 radial magnetic field produced by the EFCCs from the total n=1 radial magnetic field amplitude. When the time derivative of such compensated quantity is above the empirically determined threshold of 0.3, the RTCC system initiates the asynchronous operations of the magnetic island healing, which is a method to avoid disruptions in EF identification experiments, that will be explained in details in Subsection 3.1.2.

For the calculation of the external n=1 magnetic field, vacuum shots have been realized by feeding each EFCC pair singularly with a current ramp waveform, in order to get the transfer functions among the n=1 EFCC current and the n=1 radial magnetic field amplitude. The transfer functions obtained in this way for each n=1 EFCC pair have been then included in JET RTCC. Furthermore, by linearly combining the signals of saddle coils in opposite toroidal positions (octants 1-5 and 3-7), the sine and cosine components of the n=1 radial magnetic field amplitude of the locked mode can be extracted, thus providing the amplitude and phase of the perturbation (Figure 2.12).

Moreover, at JET [7] locked modes have seen to be peaked in the midplane (1 and 14 poloidal position loops), as expected, but also a significant signal has been observed in the ex-midplane coils, consistently with the evidences reported in DIII-D experiments [10]. This is why the locked mode detector is implemented with multiple sensor sets, based on the poloidal deformation of locked modes.

2.5.2 Beta-induced Alfvén Eigenmodes in presence of locked modes

As it has been explained in Subsection 1.4.1, when deriving the set of MHD equations if one neglects the displacement current in Ampère's law, electromagnetic waves in the plasma are not allowed. However, it has been also derived that the MHD model provides two kinds of restoring forces against a displacement of a field line, the magnetic pressure and the field line tension, that actually give rise to MHD waves, the so-called Alfvén waves.

Shear-Alfvén waves are transverse plasma waves that propagate along the magnetic field with an Alfvén velocity, $v_a = \frac{B}{\sqrt{4\pi\rho}}$, where B is the magnetic field and ρ the plasma mass density. The frequency spectrum of such waves is characterized by discrete values in the high range and a continuum in the low one. The high frequency waves are called Alfvén eigenmodes (AEs) and rotate with either $\omega \simeq \omega_a = \frac{v_a}{qR_0}$, where q is the safety factor and R_0 the torus major radius, or $\omega \simeq \frac{\omega_a}{2}$, depending on their origin. On the other hand, the Beta-induced Alfvén eigenmodes represent the low frequency component: they are due to the plasma compressibility that affects the geodesic curvature and the β parameter. Among the several scenarios in which BAEs are observed, they appeared in different devices during Ohmic discharges characterized by

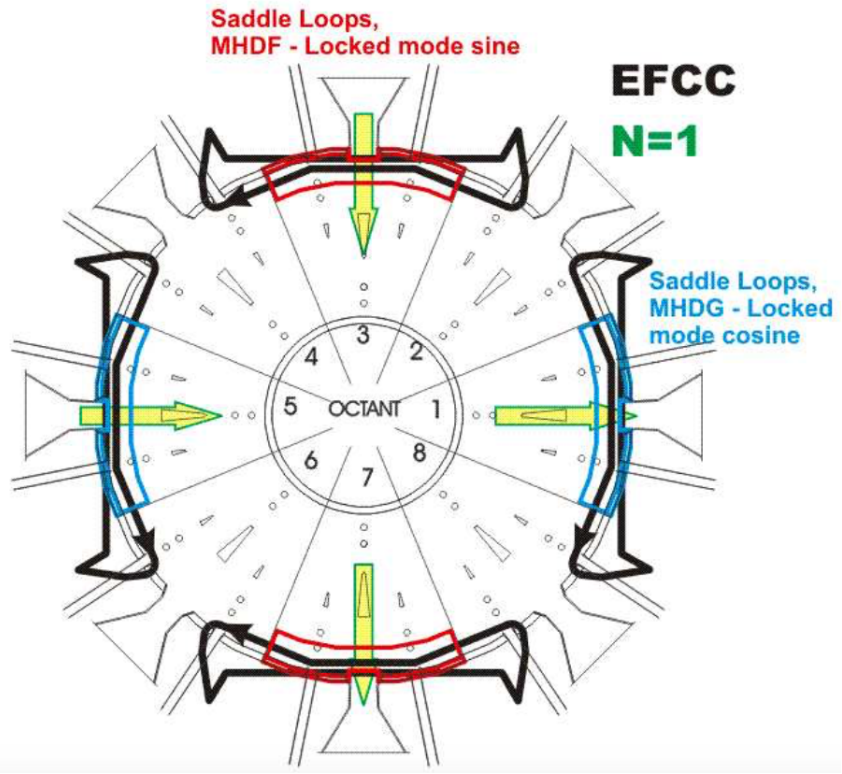

Figure 2.12: Representation of the set of saddle coils in the four octants 1,3,5,7 for the n=1 locked mode detection.

the presence of tearing modes, as MHD activity associated to the correspondent locked magnetic island [11-16]. In particular, evidences highlight that when the mode is not completely locked, two BAEs branches appear in spectrograms for every island, with frequencies that slightly differ from one another. Both branches are resonant with the island, i.e. they are characterized by the same toroidal mode number of the correspondent tearing mode, but with opposite signs, which means that one of them (the higher frequency one) rotates in the same direction of the mode, while the other (the lower frequency one) counter-rotates. The frequencies of the two branches are spaced by

$$\Delta f = 2 f_{TM} \tag{2.3}$$

where f_{TM} is the tearing mode frequency. Hence, when the mode finally locks, i.e. when $f_{TM} = 0$, Δf vanishes and the branches are no more distinguishable. Theory explains the onset of BAEs with the formation of a standing wave in rest frame of the island, from the overlapping of the two branches. The standing wave frequency is the mean between the frequencies of the branches,

$$f_{BAE} = \frac{f_{co} + f_{counter}}{2} \tag{2.4}$$

At JET [7,8], BAEs have been observed as MHD activity in Mirnov spectrograms in the range between 5 and 20 kHz, acquired during experiments of EF identification in Ohmic plasmas and during the plasma current ramp-down phase: both of these scenarios are characterized by strong tearing activity. In the shots analyzed in this thesis, BAEs signatures appear in the frequency range consistent with the literature and in a time window of few seconds. Figure 2.13 reports an evidence of BAEs associated to a TM, during a discharge at JET. In the top panel, two BAEs signature appear in the phase in which the TM frequency is rapidly decreasing. Before the locking ($\sim$ 14.6 s), they are split into two branches with opposite toroidal mode numbers, as it results from an analysis of the Mirnov array signal (second panel from the top). When the TM frequency drops below 0.1 kHz, the branches become unresolved, in fact two single signatures can

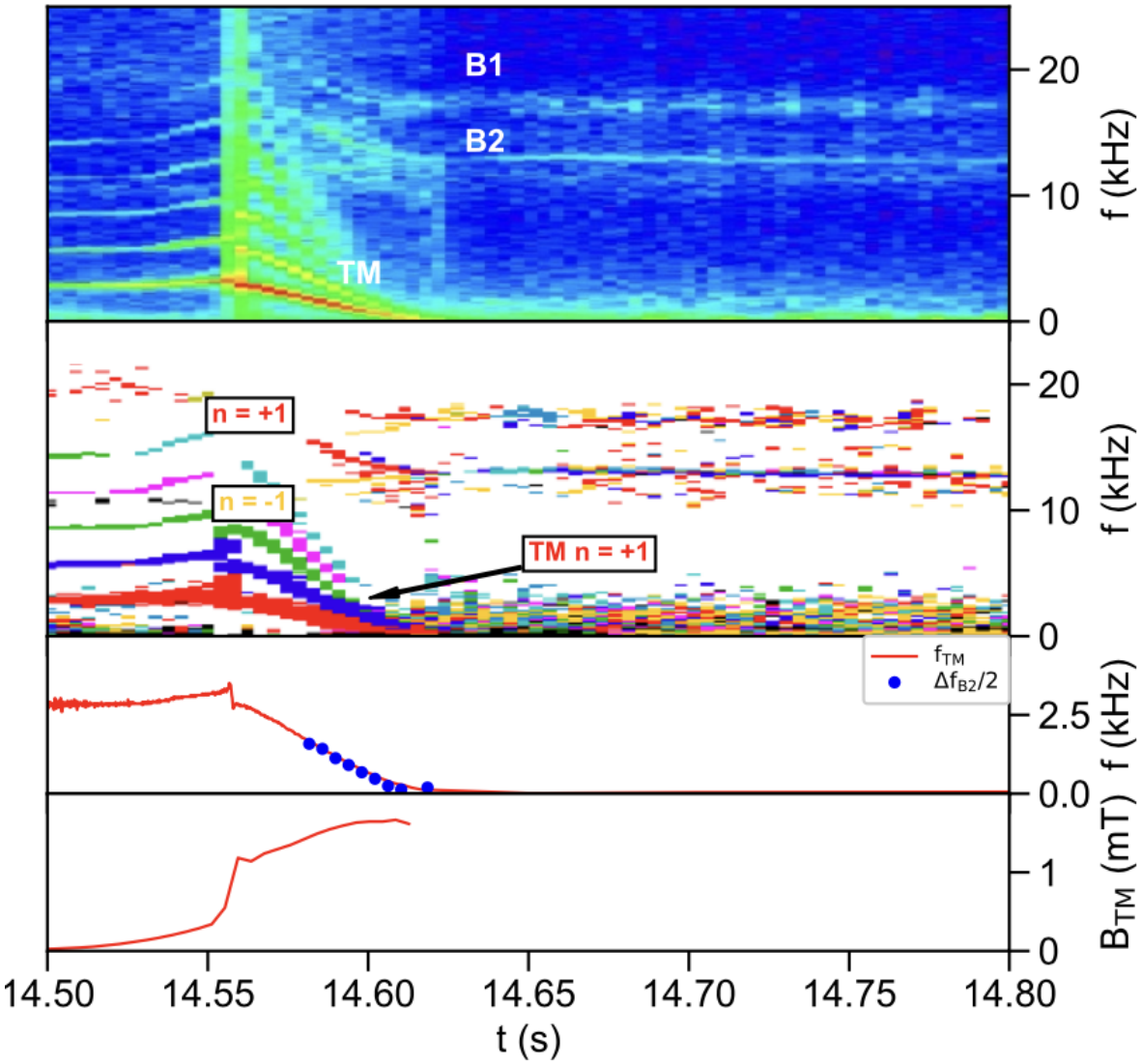

Figure 2.13: Evidences of BAEs associated to a TM at JET (JPN 97589 pulse). From top to bottom: spectrogram from a Mirnov coil; toroidal mode number analysis from the Mirnov coils array; n = 1 TM frequency (solid line), compared with the half difference between the frequencies of the two branches before mode locking (solid circles); n = 1 TM amplitude from Mirnov coils. Image taken from [8].

be seen, centred around 17 and 13 kHz. It is then instructive to see how the evolution of the n=1 TM amplitude, reported in the bottom panel, suddenly increases when the TM starts to lock.

In [7] it is also reported the evidence, consistent with the theory, that BAEs tend to disappear when their frequency reaches the continuum accumulation point (CAP): as an analogous of electronic band gap in conductive materials, the discrete frequencies of BAEs lie in a gap opened in the shear-Alfvén continuous spectrum by the finite plasma compressibility. Moreover, in several JET pulses [8] is has been found that there is a critical size for the magnetic island width to be reached in order excite BAEs activity. These facts make the use of BAEs signatures less efficient in detecting the locked mode induced during the EF identification, even though the CAP value can be calculated within a robust theoretical framework [8], which is easy to implement in JET RTCC. The mode amplitude calculation provided by saddle coils remains thus the main locked mode detection metric, to be mated with the monitoring of BAEs activity in Mirnov signals, that is usually used as a secondary evidence of the locked mode onset. However, it becomes a very important means when the saddle coil measurements are no longer available,

as sometimes happens in the late termination phase, or when it is difficult to distinguish several modes with the same toroidal mode number.

It will be clear in Subsection 3.1.2 that the locked mode detection plays a main role in the error field investigations. JET locked mode detector can be also applied in the future ITER plasma control system during EF identification experiments, scheduled for the first ITER operations.

2.6 Charge Exchange Recombination Spectroscopy

The charge exchange (CX) is an interaction that occurs between low-Z fully ionised impurities in the plasma, A^{Z+}, and injected neutral particles, H^0, when an elementary charge is exchanged through the transfer of an electron from H to A, producing hydrogen-like ions $A^{(Z-1)+}$:

$$H^0 + A^{Z+} \rightarrow H^+ + A^{*(Z-1)+} \tag{2.5}$$

This phenomenon usually leaves the produced ion in an excited state, that de-excites by emitting photons, whose spectrum can be used to extract information on the plasma. This diagnostic technique is called *Charge Exchange Recombination Spectroscopy* (CXRS). Before to the CX interaction, the impurity ions are assumed to possess the characteristics of the plasma.

From the Doppler shift and broadening observed in the CX de-exitation spectrum, it is therefore possible to obtain the angular velocity and the temperature of the plasma respectively. These are fundamental parameters for characterizing a fusion plasmas, which are measured with high spatial resolution through the CXRS. In fact, only minor uncertainties arises from atomic processes. Moreover, if the instrument has been calibrated by a light source of known radiance, the density of the impurity ions in the plasma can also be inferred. Moreover, since the CX makes the impurities to radiate locally, by changing the sight line of the spectrometer across the neutral beam path, it is possible to reconstruct the radial profiles of the measurable quantities.

The CXRS has become a routine diagnostic in almost all major thermonuclear fusion devices. At JET, the sources of neutral particles is the NBI system, which delivers atoms of the same species of the plasma ions (H isotopes). Because the higher is the atomic charge of the ions the more severe are the incurred errors, low-Z impurities are exploited: in particular, at JET the chosen elements are Helium, Beryllium, Carbon, Nitrogen, Oxygen, Neon, Argon.

The CXRS system of JET is shown in Figure 2.14. Photons from JET plasmas are collected by three separated periscopes, which transfer the light to the diagnostic room via 600 mm diameter optical fibers. Here, short focal length spectrometers are coupled to fast CCD cameras, which provide good time resolution. This system allows to observe up to six different impurity elements simultaneously.

Regarding this Thesis work, the charge exchange recombination spectroscopy has been used to measure the plasma angular velocity during EF identification studies.

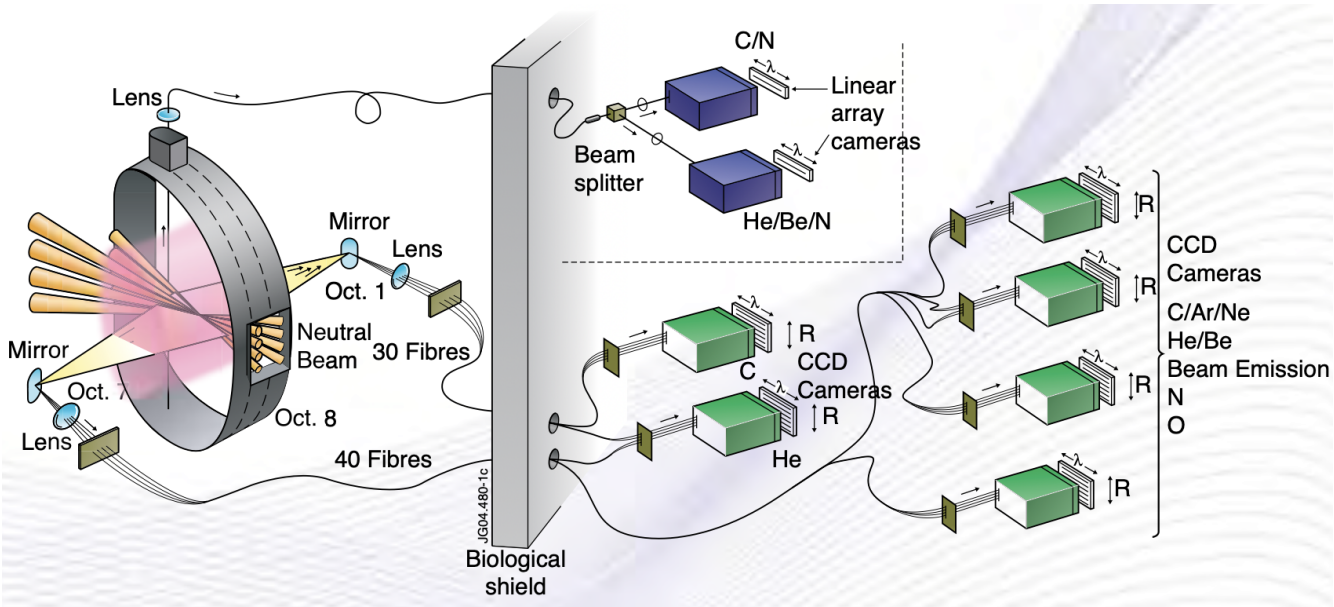

Figure 2.14: CXRS apparatus at JET: three periscopes (namely "lens") transfer the light through optical fibers to spectrometers coupled to fast CCD cameras.

Chapter 3

Rotation Braking Analysis in JET Plasmas

In this chapter, the analysis performed during this Thesis is described, the main steps are motivated by both theoretical arguments and previous evidences and the main experimental results are presented.

3.1 Error Field Identification Experiments

As described in Subsection 1.4.4, in magnetic fusion devices error fields are practically unavoidable and can lead to locked mode driven disruptions. This is a matter of concern especially for ITER, where the allowed number of disruptions will be very limited, most of all in the high plasma current regime ($I_p > 5$ MA). This is why many efforts have been made to develop techniques to identify the intrinsic error field and to suppress or, at least, to minimize it and thus avoiding the plasma disruption.

3.1.1 The standard compass scan method

The compass scan [50] is a method to identify the magnetic topology, i.e. amplitude and phase, of the error field of the machine and provides an experimental procedure for the correction of such perturbation. The technique is based on the assumption that the magnetic island formation, during the external field penetration, depends only on the amplitude of the total non-axisymmetric field, B_{tot}, which is given by the sum of the externally applied magnetic field, the non-axisymmetric component of the externally applied magnetic field and the EF. The compass scan is therefore performed during the plasma current flat-top phase, in order to avoid unwanted spurious effects. The threshold value for the field penetration should lie on a circle in the complex plane $Re(B_{tot})$ vs $Im(B_{tot})$.

The compass scan is executed by probing an external field in the plasma until a locked mode is triggered and its related magnetic island forms, by changing the amplitude and the toroidal phase of the current phasor that is used to induce the mode, I_{prob}. Indeed, because of the presence of the intrinsic error field, the current required for the external field to lock the mode varies with its toroidal position. In particular, when the toroidal phase of the probing field coincides with the toroidal phase of the EF, the locked mode onset occurs at lower values of the current, while, when the two toroidal phases are opposite, a higher current is needed to trigger the mode. All the values of the amplitude and of the phase of the current phasor set during the scan are recorded and used to realize a polar plot in the complex plane $Re(I_{prob})$ vs $Im(I_{prob})$, in which data is fitted with a circle. In the ideal situation where no EF is present, the circle is centered at

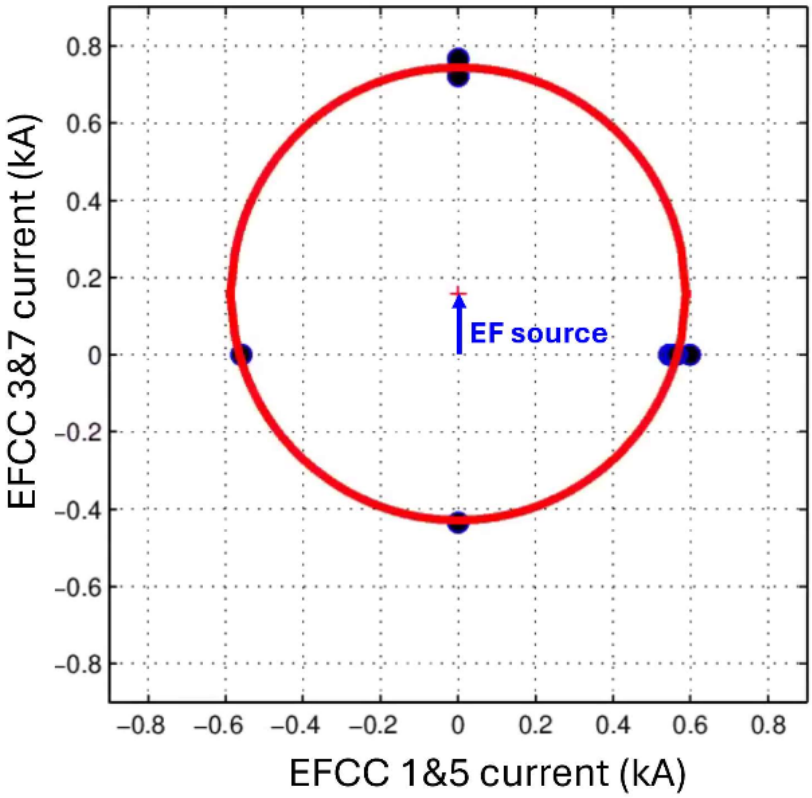

Figure 3.1: Polar plot of the EFCC currents during a compass scan in an Ohmic regime, characterized by 1.8 MA plasma current and 2.1 T toroidal magnetic field. The shifted center of the circle indicates the presence of an intrinsic error field in the machine.

the origin of the axes. In real situations, where the error field is unavoidable, the circle center is shifted from the (0,0) point and its coordinates allow to identify the EF magnetic topology.

The identification of the EF source yields the correction currents for its minimization, which can be used in a pre-programmed way during plasma operations. Furthermore, an accurate description of the EF sources allows to elaborate control strategies, based on electromagnetic modelling coupled with the plasma response, as, for example, the IPEC code [49].

At JET the EFCC system, described in Section 2.3, is exploited to induce an n=1 perturbation and its amplitude and phase are changed to accomplish the toroidal scan. In Figure 3.1 an example of the polar plot realized during a compass scan at JET [2] is presented. The shift that affects the circle centre indicates a source of EF.

EFCCs are present also in ITER and in other devices, such as MAST-U. At the beginning of ITER plasma operations, they will be used in EFs identification experiments, this is why the compass scan method has been executed in several magnetic fusion devices [50] besides JET[54, 55], such as MAST-U [56, 57], NSTX [51], ALCATOR-CMOD [52], ASDEX-Upgrade [53], EAST [58], DIII-D [59, 60], KSTAR [61] and RFX-mod [62].

The main problem related to the compass scan test, that resulted from various experiments, is the formation of locked modes induced by the current increase, which has been observed to lead to a plasma disruption both during the execution of the technique, when the plasma current is in the flat-top phase, and after the test has been ended. Both the cases are documented in [5] and represented in Figure 3.2. In particular, at the left side a MAST-U discharge is shown, in which a disruption happens during the plasma current flat-top, in correspondence of a locked mode induced by ramping the EFCC current. On the other hand, at the right side a JET discharge

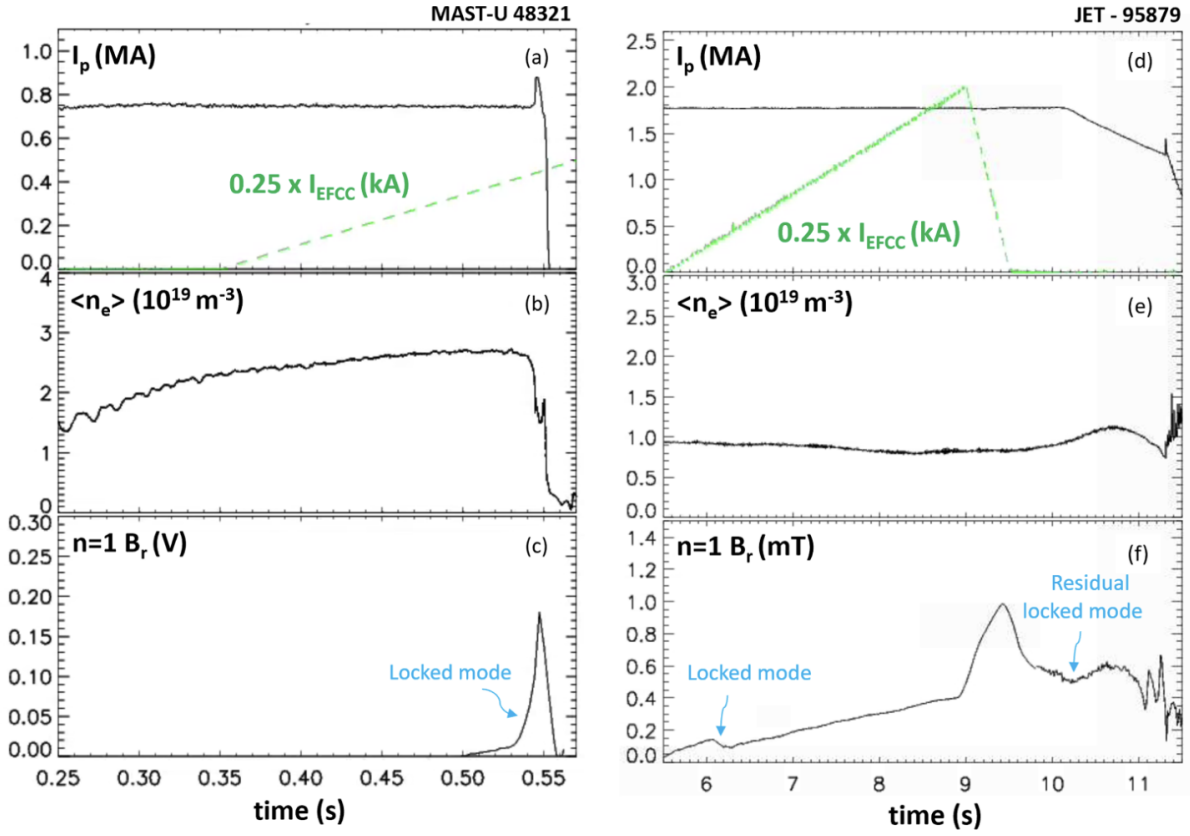

Figure 3.2: Time behaviour of (a,d) plasma current, (b,e) plasma density, (c,f) compensated n = 1 radial magnetic field during the execution of compass scan tests. On the left, data refers to a MAST-U discharge realized in an Ohmic regime with 0.75 MA plasma current and 0.5 T toroidal magnetic field. On the right, data refers to a JET discharge realized in an Ohmic regime with 1.8 MA plasma current and 2.1 T toroidal magnetic field.

shows a disruption occurring after the EFCC current has been switched off, because of the presence of a residual locked mode that originated during the EFCC ramp.

Such kind of dynamics can not be tolerated in future disruption-averse tokamaks such as ITER and this is why efforts have been made to develop a *non-disruptive compass scan* method.

3.1.2 The non-disruptive compass scan

In order to accomplish the compass scan in a non-disruptive way, a procedure called *magnetic island healing* has been established. It consists in two asynchronous operations:

i. the EFCC current is switched off quickly as soon as the locked mode onset is detected;

ii. the plasma density is raised by the operator in a controlled way.

After the operation (i), the driving effect on the island is removed and in the meanwhile the density is increased. Indeed, the density raise implies an increase of the plasma viscosity and inertia, which means an increase of the viscous coupling between the island and the plasma that flows around it. This viscous torque forces the island to rotate against the electromagnetic (EM) one driven by the residual EF. This means that, if ideally the intrinsic error field could be completely suppressed, no density increase would be necessary.

This phenomenon has been modeled in [5] through the RFXlocking cylindrical code [63], adapted to JET geometry and implemented with the EFCCs contribution. The model is based on the description of the island width in a twofold regime. In particular, during the EFCC ramp, the linear resistive-viscous regime is established, in which the island begins to form due to the finite resistivity, that allows to tear and recombine the magnetic field lines. After the penetration at the resonant surface, marked by a steep increase of its width, the island enters in the Rutherford non-linear regime where the no-slip constraint holds, which means that the island is frozen within the electron fluid at the resonant surface. In Figure 3.3 the island evolution during the execution of the non-disruptive compass scan is simulated. The EFCC current in the Rutherford regime is kept at a finite value to mimic the presence of an intrinsic residual EF (panel (a)).

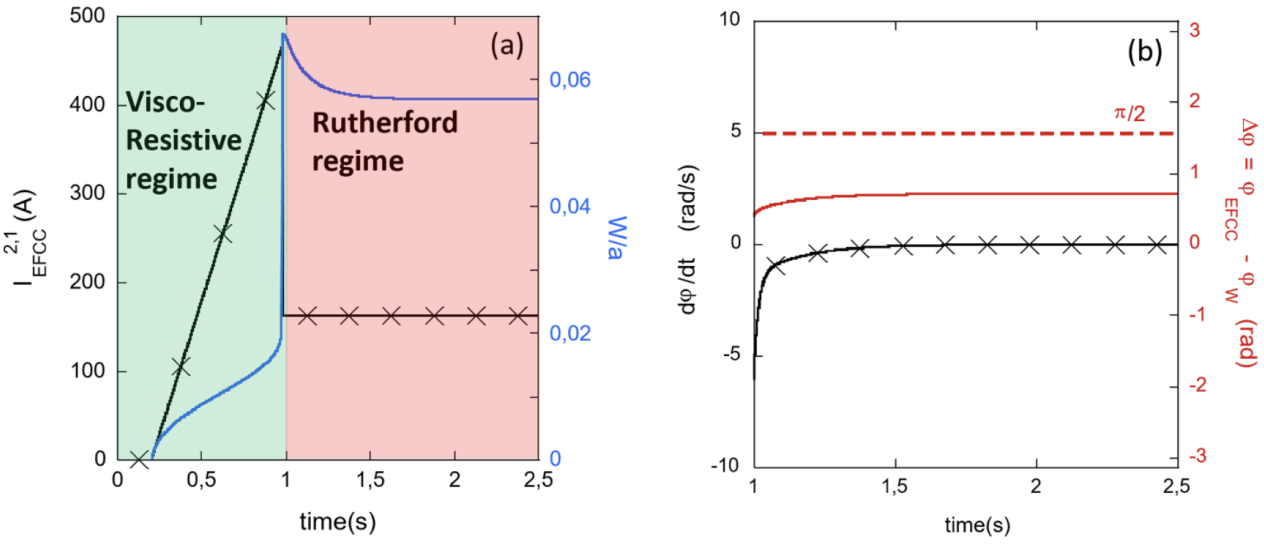

Figure 3.3: (a)Time evolution of EFCC current (black) and normalized island width (blue). (b) Island phase velocity (black) and the difference between the island and EF phases in the Rutherford regime (red).

The finite shift between the island and the EF phase simulated in panel (b) has been actually

observed and it comes from the balance between the electromagnetic and the viscous force. In terms of torque equilibrium, the balance equation reads

$$const \times |I_{EFCC}| W^2 sin(\Delta\phi) = -\rho\nu\omega_0 \tag{3.1}$$

where ρ is the mass density, ω_0 the island angular frequency under no EM torque and W the island width. The left side represents the EM torque, the right side the viscous one. For fixed values of I_{EFCC} and W, equation 3.1 implies that, if the viscous force increases, at the left side $\Delta\phi$ approaches $\frac{\pi}{2}$, up to the situation in which, at $\Delta\phi = \frac{\pi}{2}$, a further increase of the viscous torque makes the balance no more valid, thus allowing the island to rotate. Therefore, if ν and ω_0 are not altered, raising the density brings to a spin-up of the locked island, hence a stabilization of the perturbation.

The non-disruptive compass scan has been designed and tested in DIII-D and executed also at MAST-U, to assess its feasibility in magnetic fusion devices, as documented in [6], [5] respectively.

In order to execute the non-disruptive technique, a magnetic fusion device must be provided with a robust locked mode detection system, whose fundamental role is to trigger the two asynchronous operations that allow the magnetic island healing, quickly after the detection. Figure 3.4 shows an example of the execution of a non-disruptive compass scan at DIII-D, depicting the described procedure. Field penetration is detected in real-time by looking at the time evolution of the midplane poloidal/radial magnetic field phase (panel (b)). After a short time delay, needed to make the penetration effective, the EFCC current is terminated (panel (a)) and the density is asynchronously increased (panel (c)) by gas puff injection. It is important to stress that, if the magnetic island healing is accomplished too early, the locked mode is not triggered and the experiment is useless.

Here comes the fundamental role of the JET locked mode detector described in Section 2.5, which is indeed exploited while performing such experiments. Although the non-disruptive compass scan requires a more sophisticated real-time control system than the conventional technique, it is far more advantageous in disruption-adverse fusion devices, not only because it actively prevents the disruptive scenario, but also because it reduces the number of pulses needed for EF identification, thanks to the multiple error field penetration threshold measurements per pulse allowed by the prompt locked mode detection and island healing.

All the shots analyzed in this thesis have been realized by executing the non-disruptive compass scan two times, while acquiring rotational measurements both during the EFCC ramp phase and the magnetic island healing. The density increase has been obtained either by gas puff or pellet injection.

Figure 3.5 shows the example of the shot 103324, which has been taken in an Ohmic regime, with 1.8 MA plasma current (panel (a)) and 2.1 T toroidal magnetic field. The two compass scans have been executed by ramping up the EFCC current up to 900 A (panel (c)). When the error field penetration occurs, the locked mode onset is observed as a growing n=1 radial magnetic field perturbation on the saddle coils data (panel (d)). This dynamics is detected in real time by the locked mode detector which eventually initiates the asynchronous EFCC/density control. Indeed, the plasma density (panel (b)) has been increased by massive gas injection, after the termination of the EFCC current (panel (c)). In order to heal the island in a successful way, it has been observed [6] that there is a density threshold below which the mode persists. In particular, as reported in [5], the locked mode is stabilized when the density is increased at least of the 15%, which can be reached by gas puff or pellet injection. The latter is in general the preferable way, since it can be accomplished in a faster time scale and with a better particle penetration. At the same time, it is also important to not increase the plasma density above the Greenwald limit, for guaranteeing a safe operative scenario (Figure 3.5 b).

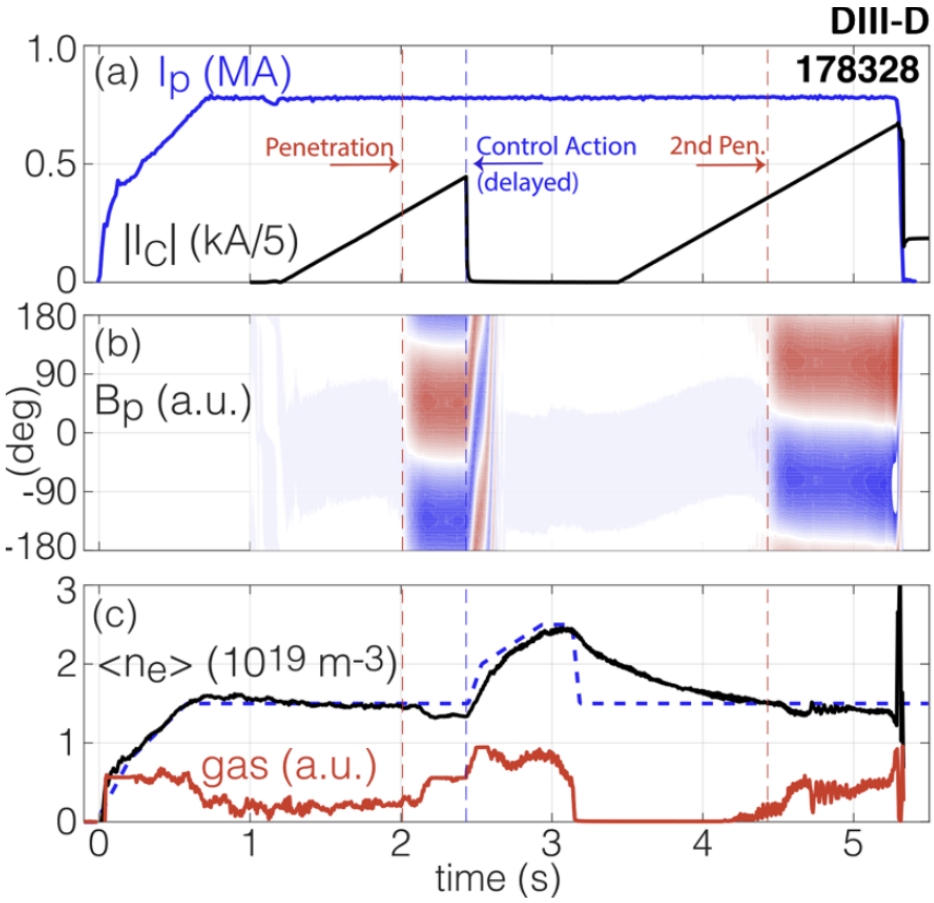

Figure 3.4: Time evolution of (a) plasma current, (b) outboard midplane poloidal/radial magnetic field and (c) density of DIII-D non-disruptive compass scan test performed in DIII-D.

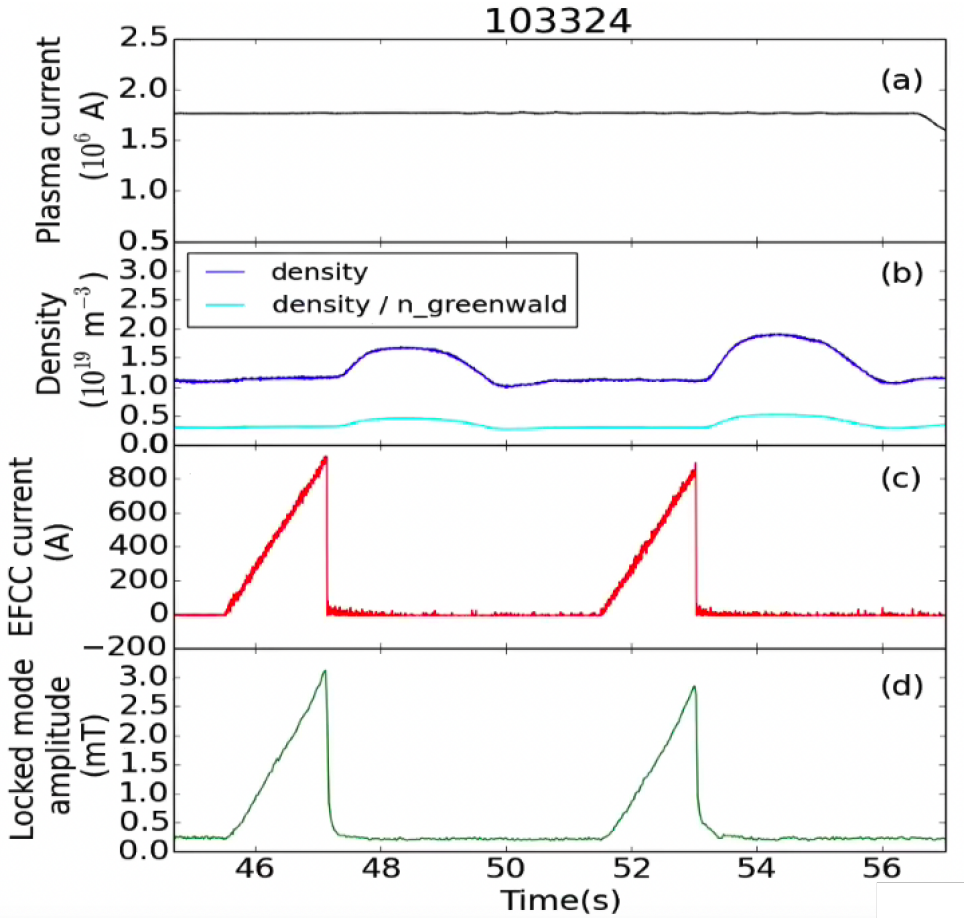

Figure 3.5: Time evolution of (a) plasma current, (b) plasma density (blue) and plasma density normalized to the Greenwald limit (cyan), (c) EFCC current, (d) amplitude of the externally induced locked mode during the realization of two compass scans. Data refers to the 103324 discharge, taken in an Ohmic regime with 1.8 MA plasma current and 2.1 T toroidal magnetic field.

3.2 Rotation Braking in presence of an induced n=1 Locked Mode

The plasma rotation in magnetic fusion devices is, in general, a result of the combination of an external contribution, such as the NBI, with an intrinsic one, whose presence has been detected in absence of externally applied momentum. A complete explanation of the intrinsic contribution to the plasma rotation has not been found yet, but, according to most of the theories, it is due to internal mechanisms in the plasma itself, such as a turbulent redistribution of momentum in the core [66, 72].

The observed rotation is actually in the toroidal direction, as the poloidal contribution is strongly damped by the neoclassical viscous force, that is due to collisions between plasma particles, enhanced by the non-axisymmetric intrinsic perturbation [73,74].

Investigations on the intrinsic plasma rotation have been carried out in the years, since it is expected to be crucial in future magnetic fusion devices, such as ITER, in which the external momentum delivered in input will be quite small. Indeed, it is known that the plasma rotation plays a role in preventing disruptions, thanks to its capability of reducing or even suppressing both macroscopic MHD and turbulence instabilities, thus improving the thermal confinement and the fusion reaction rate. However, it has been also observed several times that the presence of locked modes in the plasma is responsible for a decreasing of its rotational velocity. This is explained by the fact that, as the plasma cannot flow at any significant rate through the large magnetic island associated to the locked mode, they brake the plasma rotation at the resonant surface where the island has formed, leading also to an appreciable slowing down of the plasma as a whole due to viscous coupling. A more rigorous theoretical view of this mechanism is proposed in Section 3.4. Locked modes thus spoil the beneficial functions of the plasma rotation and this is why experiments are carried out with the aim to investigate the behaviour of the plasma rotation in presence of such perturbations.

In the last campaign of JET in 2023, several shots have been realized, while applying an n=1 magnetic field perturbation by means of the EFCC system, during the execution of the non-disruptive compass scan technique. Rotational data has been acquired through the charge exchange recombination diagnostics, described in Section 2.6, with the spectrometer KS5, which exploits Helium, Beryllium, Neon, Carbon, Nitrogen impurities [47]. In order to assess the behavior of the intrinsic plasma rotation in presence of the locked mode, NBI is delivered in blips, such that its contribution to the overall plasma angular momentum is negligible. Measurements have been taken in two plasma scenarios:

- during the execution of the non-disruptive compass scans, by triggering and external n=1 locked mode ramping up the EFCC current and keeping the plasma density constant. In the following, I will refer to the accomplishment of the two techniques as CS1 (compass scan 1) and CS2 (compass scan 2);
- during the magnetic island healing procedures that have followed both CS1 and CS2, executed by switching off the EFCC current and increasing the plasma density. In the following, I will refer to them as ACS1 (after compass scan 1) and ACS2 (after compass scan 2).

For every shot, measurements of the NBI power, EFCC current, plasma density and toroidal angular velocity during the NBI blips are available as functions of time. Angular velocities have been also measured at different radii.

By means of a Python algorithm,

- the time intervals of the NBI blips have been obtained, which correspond to the time

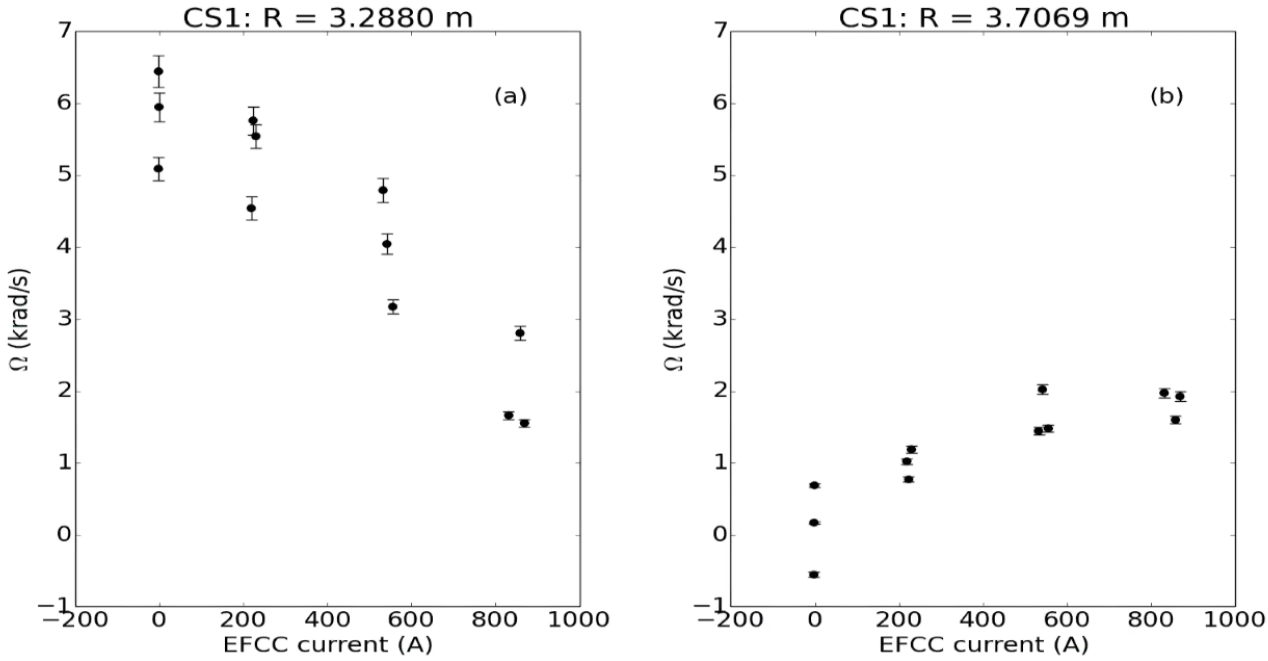

Figure 3.6: CS1 experimental results. The mean angular velocities are plotted for every NBI blip versus the EFCC current values in the middle of the correspondent time interval, making a comparison between the results in the plasma core (a) at the plasma edge (b).

intervals in which rotational measurements have been taken;

- the EFCC current values in the middle of them have been extrapolated;
- the toroidal angular velocities have been averaged in each time interval and for every radius;
- the corresponding error has been calculated using the error propagation formula, provided ax experimental uncertainty equal to the 10% of the measurement.

The averaged velocities have been plotted against the EFCC current values in the middle point of the correspondent time interval for every radial position, merging together the results of all the shots.

In Figure 3.6, the analysis performed for the first compass scan is presented. In panel (a), the experimental results obtained for a radius in the plasma core (R = 3.2880 m) show a braking of the plasma toroidal velocity with the increasing EFCC current, that is with the increasing amplitude of the induced locked mode. In panel (b), it is observed that in the case of the external radius (R = 3.7069 m) the angular velocity spins up. These evidences are consistent with the theoretical framework, which states that a significant braking happens at the resonant surface and in its neighbourhood, which is located, in this case, in the core, whereas the furthest regions, i.e the edges, are not affected and a spin up with respect to the resonant surface occurs.

In Figure 3.7 the experimental results related to the second compass scan are reported, together with the analysis of the first one, shown in Figure 3.6. Consistently with the previous figure, data is shown in the core in panel (a) and at the edge in panel (b). In the case of the second compass scan, the averaged angular velocities in the core are significantly less reduced than in the case of the first one, indicating that the density perturbation accomplished during ACS1 played a role in affecting the rotational braking.

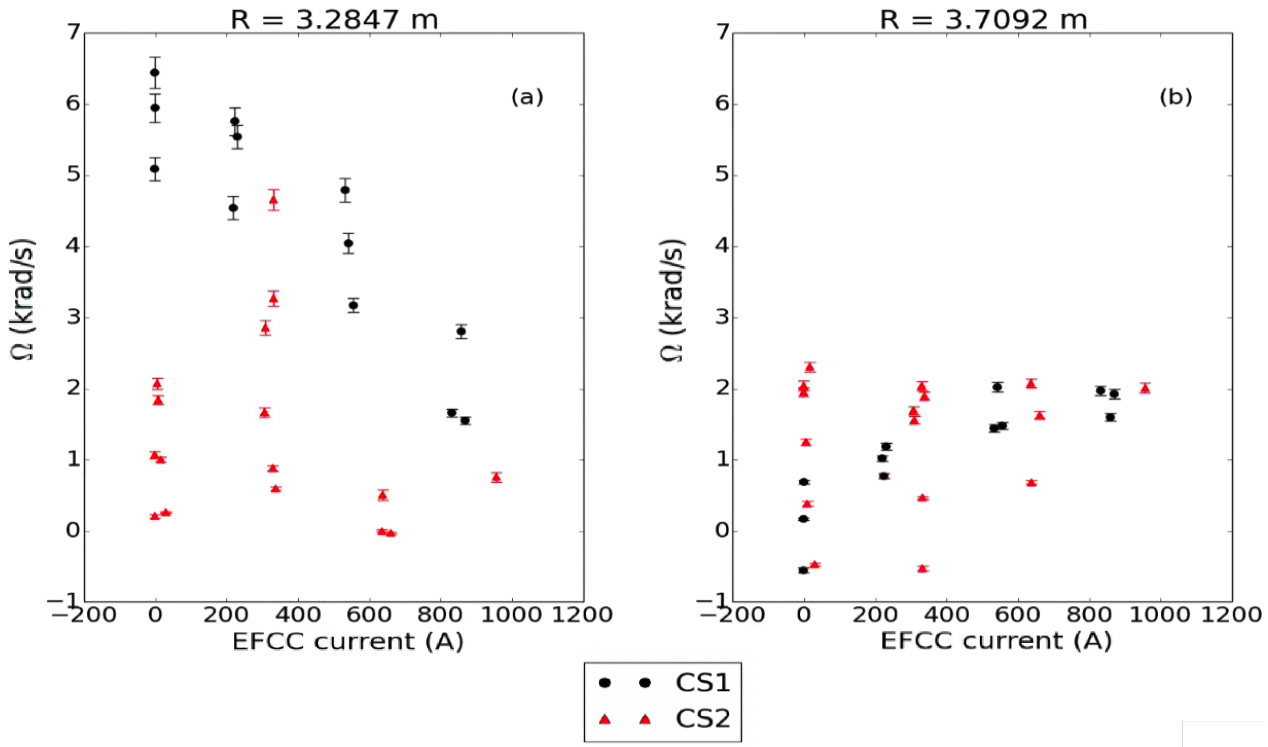

Figure 3.7: Averaged toroidal angular velocities vs EFCC currents in the middle of the correspondent time intervals. A comparison between CS1 (black points) and CS2 (red triangles) in the plasma core (a) at the plasma edge (b) is presented.

3.3 Effect of Density on Plasma Rotation

The same analysis has been performed for the magnetic island healing after both the compass scans and it is reported in Figure 3.8. In panel (a) the experimental results show a linear increase of the rotation with the increasing density in the core, indicating that the rotation braking effect, caused by the external locked mode, can be successfully stabilized by the density raise. In panel (b) the rotation value at the $q = 2$ resonant surface remains flat for both ACS1 and ACS2, as during both the compass scans.

As it is reported in [3], at JET for the first time an investigations on hydrogen, deuterium and tritium plasmas in an Ohmic regime has been carried out, in which the toroidal angular velocity in the core was measured in a wide range of densities for the three ions. It was important to clarify the possible dependence of the plasma rotation on the isotope type, since future fusion devices will work with both deuterium and tritium. They restricted the analysis in the radial range of the core, because it had been observed that the angular toroidal velocities of H, D and T plasmas were appreciably different only within this region, for a fixed plasma density. It has been found out that, as the density was increased, the same trend was followed by the three isotopes, that is a changing of the rotation radial profile from a peaked to a hollow profile and then again to a peaked one.

The same phenomenon has been observed also in the shots analyzed in this thesis, during the density increase executed for the magnetic island healing. Figures 3.9 and 3.10 show the examples of ACS1 (shot 103325) and ACS2 (shot 103324) respectively, both of them taken in an Ohmic regime, with plasma current 1.8 MA, toroidal magnetic field 2.2 T. As far as Figure 3.9 is concerned, comparing the NBI blips interval in panel (a) with the density profile in panel (b), it is possible to see that the density is decreasing from the black blip to the magenta one, after which it is kept constant, indicating that the magnetic island healing is terminated. In panel (c),

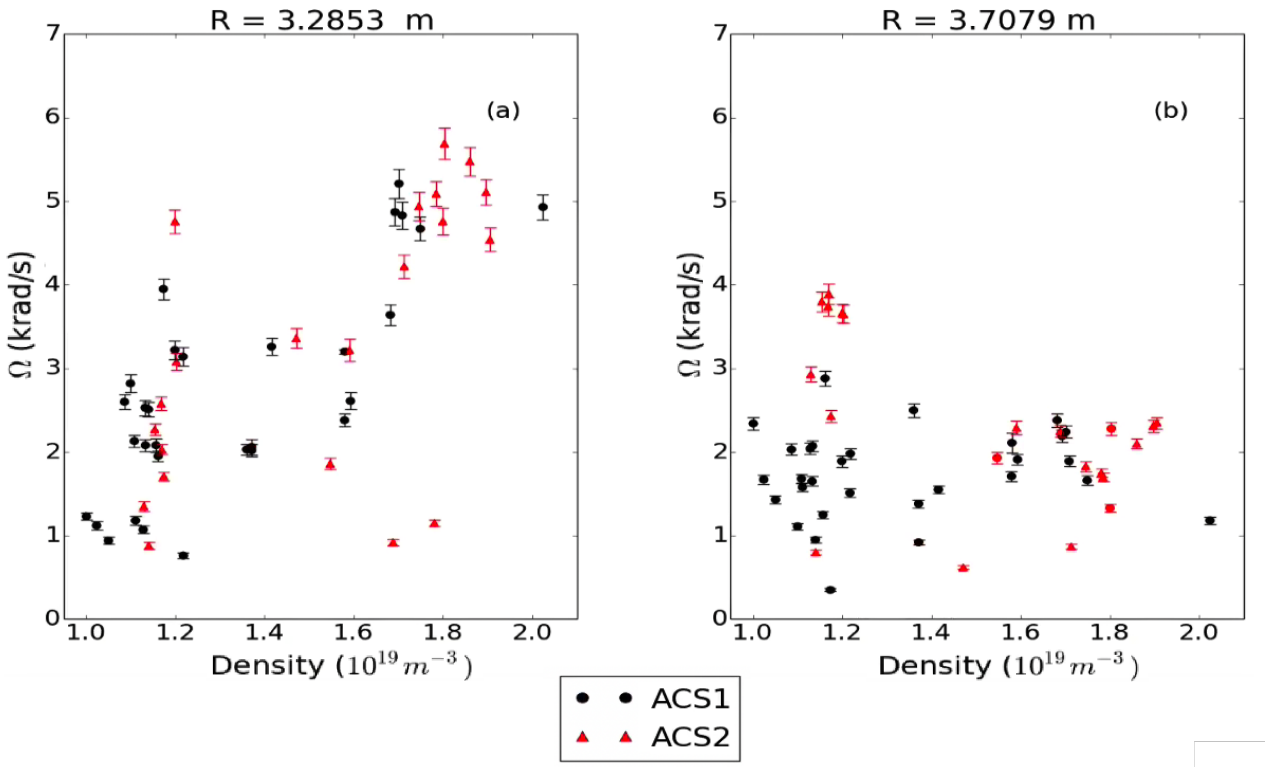

Figure 3.8: Averaged toroidal angular velocities vs plasma densities in the middle of the correspondent time intervals. A comparison between magnetic island healing after the first compass scan (black points) and after the second one (red triangles) in the plasma core (a) at the plasma edge (b) is presented.

the radial profiles of the averaged toroidal angular velocities are shown for the four NBI blips time intervals, by matching the colours with panel (a). The black and the red curves refer to the profiles acquired during the magnetic island healing, where the black one corresponds to the highest density. The magenta and green curves have been taken when the density increase had been lowered again to its flat top value. Considering the plasma core, that is the radial range around about 3.2 m, it is possible to note that the black curve displays a peaked profile, while for the other three the profile is hollow. This experimental evidence reproduces the second change of profile highlighted in [3], that is the hollow-to-peak transition of the core rotation, that occurs while increasing the density. The same trend is observed in the ACS2 case, reported in Figure 3.10, where the pink and green curves, correspondent to the highest densities, show a peak profile in the core, while the black and red curves, correspondent to the lowest densities, display the hollow profile. In both the cases, at the plasma edge neither significant differences in the angular velocities nor a transition in the rotation profile are observed, consistently with [3]. By looking at different shots, the density value at which the rotation profile transition in the core occurs is identified around 1.7 $\times 10^{19}$ m^{-3}.

Moreover, in [3] it has been observed that, while in the case of the hydrogen plasma the average angular velocity remained positive, in the case of deuterium and tritium plasma it reached negative values in the hollow profile regime, indicating a changing in the sense of the plasma rotation. Regarding the case of the present work, where all hydrogen isotopes have been used, in most of the analyzed shots the toroidal velocity is observed to change sign in the ACS1 case.

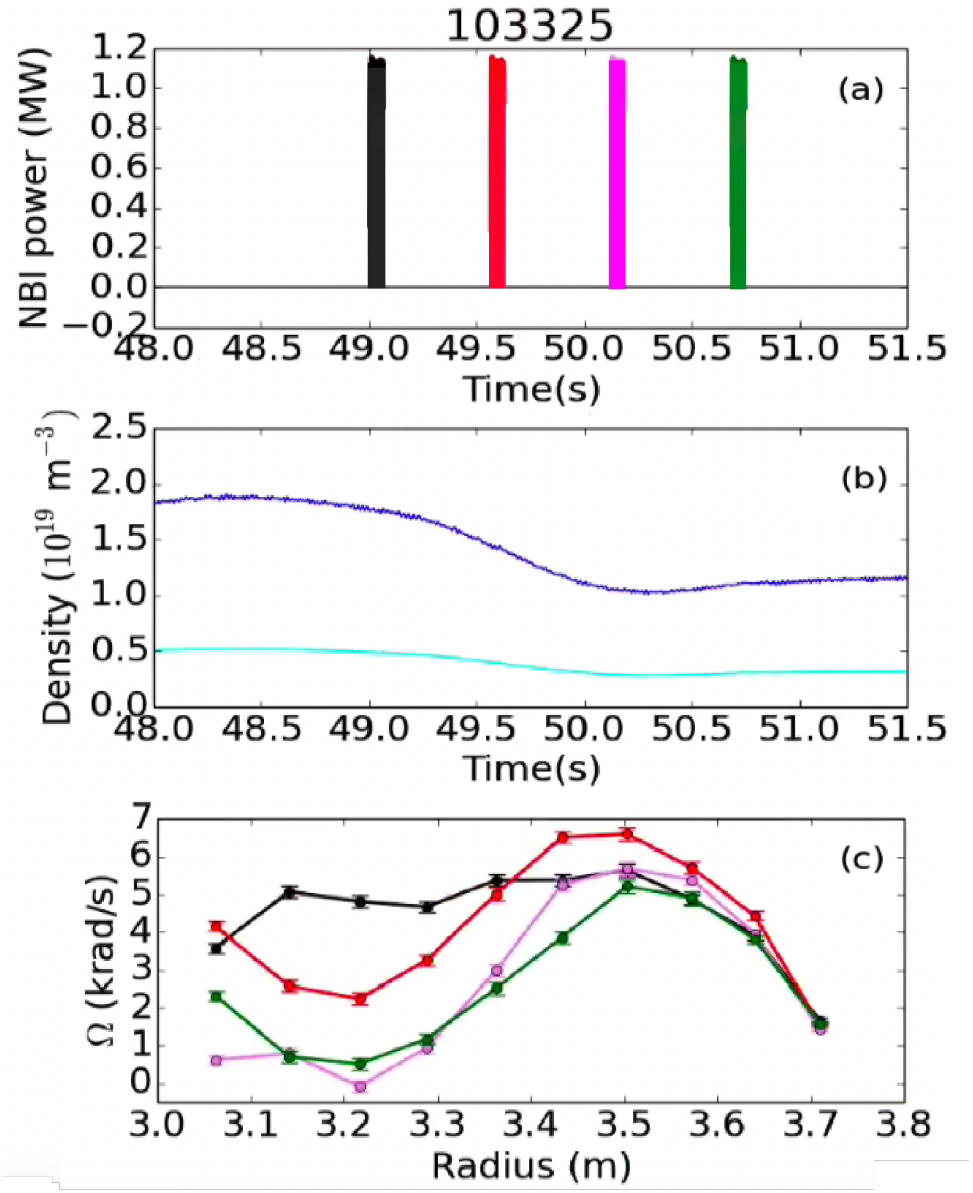

Figure 3.9: Time evolution of (a) NBI power, (b) plasma density in blue and the Greenwald fraction in cyan, (c) radial profile of the averaged toroidal angular velocities. Data refers to ACS1 of shot 103325, realized in an Ohmic regime, with plasma current 1.8 MA, toroidal magnetic field 2.2 T. The colours in (c) match the ones used in (a).

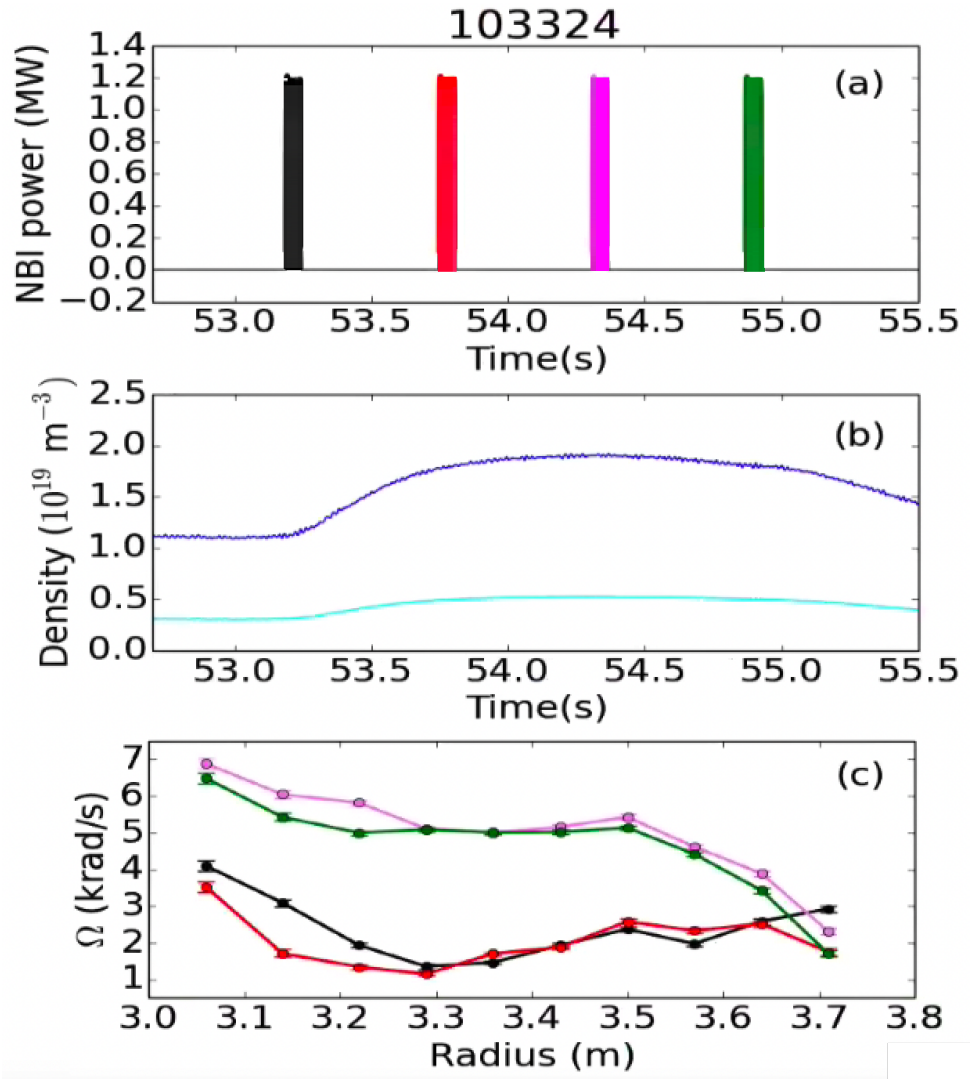

Figure 3.10: Time evolution of (a) NBI power, (b) plasma density in blue and the Greenwald fraction in cyan, (c) radial profile of the averaged toroidal angular velocities. Data refers to ACS2 of shot 103324, realized in an Ohmic regime, with plasma current 1.8 MA, toroidal magnetic field 2.2 T. The colours in (c) match the ones used in (a).

3.4 Role of Plasma Rotation in Error Field Shielding

Is Section 3.1, it has been described that the second operation of the magnetic island healing, that it the density raise, is necessary to stabilize the perturbation, since the intrinsic error field can lock the island leading to a disruptive scenario.

From a theoretical point of view, the need for a density increase is based on the principle of the enhancement of the viscous coupling to the island, that makes it to rotate against the error field braking effect. This is also supported experimentally by the fact that that there is threshold in the amplitude of the external field for the penetration to occur, that increases with increasing the density. At JET [4], the following scaling law has been investigated:

$$\frac{b_{pen}}{B} \propto n^{a_n} B^{a_B} \omega_0^{\eta}, \tag{3.2}$$

where n is the plasma density, B the magnetic field and ω_0 the plasma initial angular velocity. The best fit results obtained in [4] are

$$\begin{cases} a_n = 0.7 \\ a_B = -1.3 \\ \eta = 0.5 \end{cases} .$$

Moreover, Equation 3.2 suggests that, in principle, even a sufficiently high plasma rotation can oppose to the braking driven by the error field on the island by enhancing the penetration threshold, without the need to increase the density. Indeed, tearing modes are usually observed to rotate in the electron drift direction, that is, for a helical perturbation, a rotation counter to the one of the plasma at equilibrium.

A simple and efficient way to increase the plasma rotation is the injection of neutral beams along the tangent to the plasma boundaries, which represents an external source of angular momentum. In general, in absence of any externally applied magnetic perturbation, the momentum balance of the plasma is reached when

$$D(L_0) + T_{source} = 0, \tag{3.3}$$

where $D(L_0)$ is the momentum radial diffusion evaluated at the initial angular momentum, L_0, while T_{source} is the source term, which represents the torque given by the plasma rotation, including both the intrinsic and the external contribution, i.e., in this case, the tangentially injected neutral beams. When a 3-D magnetic field perturbation is applied, a change in the angular momentum happens, $\Delta L = L - L_0$, and the momentum balance equation takes the form

$$\frac{\partial L}{\partial t} = D(\Delta L) + T_{NTV} + T_{j\times b} + T_{Rey}, \tag{3.4}$$

where T_{NTV} is the *neoclassical toroidal viscous torque*, $T_{j\times b}$ the *resonant electromagnetic torque* and T_{Rey} the contribution coming from the *Reynolds stress tensor*. Equation 3.4 is valid under the assumption that the 3-D perturbation does not affect the momentum diffusion coefficient, which represents the main contribution in the expression of $D(L)$, nor the source term. $T_{j\times b}$ is associated with shielding currents that are generated at the resonant surfaces, hence it is characterize by a local nature and it is responsible for the local rotation braking experienced by the plasma. The T_{NTV} is present only in non-axisymmetric plasmas and it appears when the amplitude of the external 3-D magnetic perturbation becomes significant. In principle, the magnetic field associated to the symmetry breaking, that is the error field, is a second order perturbation, but, if at the rational surface a magnetic island of finite width originates, the order of magnitude of the symmetry breaking effects is expected to raise. In particular, the non-resonant component of the intrinsic EF gives rise to the neoclassical toroidal viscous torque.

Provided its global nature, it is a good candidate to explain the global anomalous braking of the plasma rotation, that has been observed in [4]. Finally, the T_{Rey} is a result of the plasma inertia, the perturbed velocity and the stochastization of the field lines.

The aim of this second part of the analysis is to investigate whether the NBI system can actually oppose to the braking torques that originate from the presence of the locked mode, resulting during the execution of the compass scan technique.

In the last campaign of JET, shots have been realized by performing the compass scan and delivering NBI power both before and during its accomplishment. The same 3-D magnetic field perturbation has been applied in all the shots, by ramping up linearly the EFCC current. The NBI power values have been chosen such that the plasma is kept in the low confinement regime (L-mode). This is required in order to avoid the MHD activity of the Edge Localized Modes (ELMs), associated to the high confinement regime (H-mode), that develops in a higher range of the external heating power. The plasma density has been kept constant throughout the duration of the compass scan.

In panel (a) of Figure 3.11 the described operative scenario is presented, by showing the example of the shot 103327, realized with 1.8 MA plasma current and 2.2 T toroidal magnetic field. The four shots considered during this part of the analysis are shown in Figure 3.12, together with the correspondent NBI power value, that are 0.5, 0.8, 2.3, 3 MW. For the shot 103697, NBI has been delivered in two delayed time intervals with different power values.

Measurements of the angular velocities have been acquired at different radii, during the time interval in which the neutral beams have been injected, through the charge exchange recombination spectroscopy.

By means of a Python algorithm,

- four time instants during NBI delivering have been chosen both before and during the EFCC ramp;
- angular velocities have been averaged over a range of 20 ms around these instants for every radius.

In Figure 3.11, panel (b) depicts the radial profile of the obtained averaged toroidal velocities for the shot 103327: the blue and red curves represent the four averages at the four time instants chosen, respectively, before and after the EFCC ramp. It is observed that the curves are not significantly different from each other, indicating that the NBI system is able to give to the plasma a sufficient amount of angular momentum, that shields the braking effect on the rotation. The same results is found for all the analyzed shots.

In Figure 3.12 a comparison between the analysis performed on the compass scan measurements in the first part and in the second one is presented. In particular, in panels (a,d) the green dashed line represent the EFCC current ramped during the execution of CS2 for the shot 103324; the correspondent NBI blips are shown together with the NBI power delivered during the shots analyzed in the second part. As it has been said above, two compass scans have been executed for the shot 103697, hence the time axis of all the quantities of all the shots depicted in Figure 3.12 has been shifted to the time interval correspondent to the first compass scan of 103697, in order to compare them better. In panels (b,e) it is possible to see that the plasma densities are kept constant during the execution of the correspondent compass scans. Panels (c,f) show that the angular velocities are constant in time for the shots in which the NBI has been delivered continuously, while the rotation braking of the plasma core is observed in the case of the shot 103324 (green dots). In order to visualize it better in the graph, the averaged angular velocities of 103324 are multiplied by 10, hence they are actually lower than in the other cases, both in the core and at the edge, as it is expected. This evidence highlights that even the lowest NBI power,

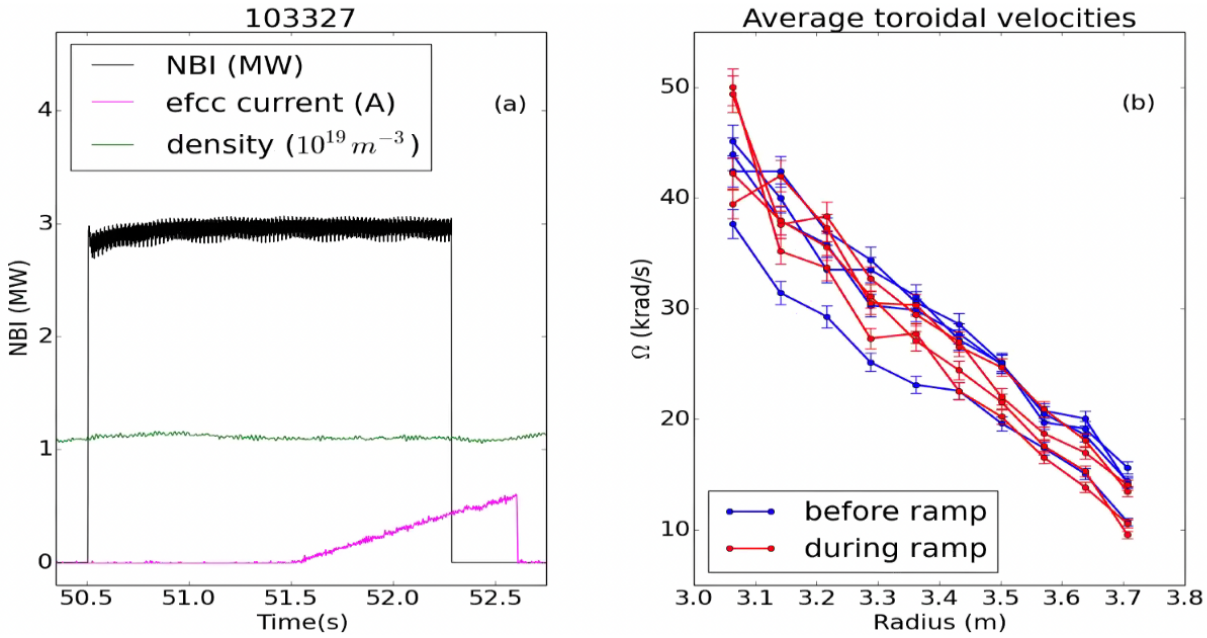

Figure 3.11: (a) Time evolution of NBI power (black), EFCC current (magenta), plasma density (green). The neutral beams are injected both before and during the EFCC ramp, while keeping the density constant. (b) Radial profile of the averaged angular velocities around four time instants before (blue) and during (red) the EFCC ramp. data refers to shot 103327, taken in a non-Ohmminc regime (3.0 MW NBI power), with 1.8 MA plasma current and 2.2 T toroidal magnetic field

i.e. 0.5 MW, is able to prevent the field penetration, being the rotation about 10 times higher in this case with respect to the results obtained for the discharge 103324.

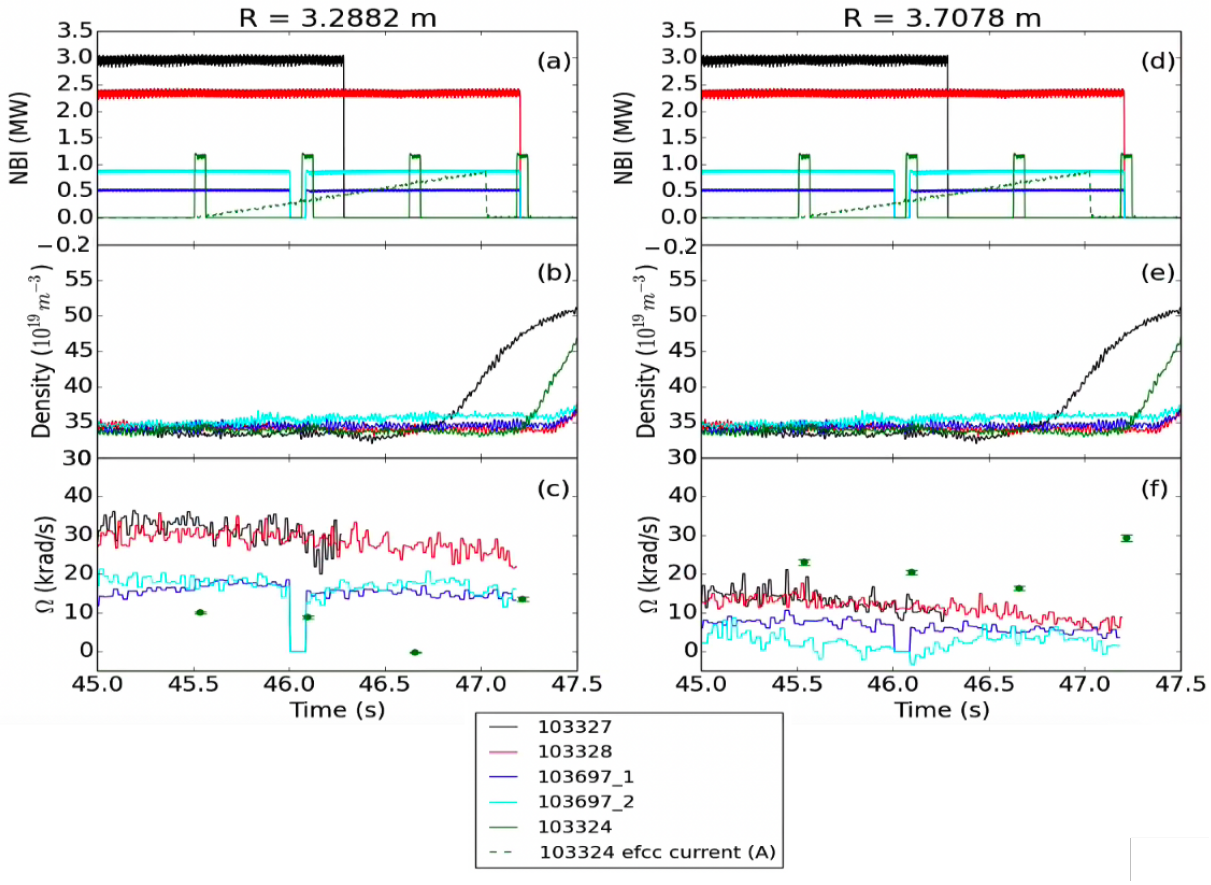

Figure 3.12: Time evolution of (a,d) NBI power, (b,e) plasma density, (c,f) angular velocity in the core and at the external radius respectively. The black, red, blue and cyan curves refer to the shots considered in this second part of the analysis, while the green dots represent the results of CS2 (first three points) and ACS2 (last point) for shot 103324. In panels (a,d) the green dashed line refers to the EFCC current ramp during CS2 for the shot 103324.

Conclusions

In this Thesis work, the rotation braking in presence of externally induced locked modes has been observed and analyzed, considering a set of experiments carried out at JET in 2023, while performing the non-disruptive compass scan technique, which is a safe method to identify the error field intrinsic of the machine.

This method will be used in ITER and next step fusion devices, which can tolerate a low number of disruptions.

Data has been acquired in the low rotation regime, that is an interesting ITER relevant regime, while ramping up the current in the EFCCs system in order to perform the error field identification. This procedure has been repeated two times (CS1 ad CS2), each of them followed by the related magnetic island healing to avoid the risk of disruption.

In this context, the interplay between plasma rotation and externally applied 3-D fields has been investigated. The main insights that have been gathered during this thesis work are summarized in the following.

- The rotation is affected by the presence of a locked mode in the plasma core, which is observed to brake, while at the edge the plasma spins up. This evidence is highlighted during CS1, whereas during CS2 the plasma angular velocity profile remains almost flat, indicating that the density perturbation applied during the magnetic island healing between CS1 and CS2 had played a role in affecting the braking.

- The rotation is affected by the density. Indeed, during the magnetic island healing executed after the two compass scans, plasma rotation in the core is not braked, demonstrating that such a technique is actually able to suppress the locked mode onset. Moreover, a changing from a hollow to a peak profile in the angular velocity while increasing the density has been observed in the core, but not at the external radius, which is in agreement with previous findings.

- The rotation is affected by the NBI, in fact the profile remains flat in presence of an externally induced locked mode. The NBI is therefore able to shield the field penetration thus avoiding the braking, even without increasing the density.

The investigation carried out in this Thesis can be extended to discharges realized in other devices. For example, at MAST-U [30,31] the same dynamic has been observed, i.e. a locked mode has been triggered when the plasma rotation was below a threshold value. Moreover, both at JET and at MAST-U, rotation data has been acquired also in presence of naturally triggered locked mode. These databases represent an important possibility to investigate the mechanism behind the rotation braking, e.g., by identifying scaling laws that relate the locked mode physics with the plasma rotation. This would bring a significant contribution for one of the main goals of the International Tokamak Physics Activity (ITPA) [42], that is the control of MHD activity to avoid disruptions ("MHD, Disruption and Control").

In order to validate the analysis, the experimental results should be finally compared with codes that solve the momentum balance equation, such as the MARS-Q [75].

Bibliography

[1] L. Piron *et al*, On the use of error field correction coils in JET, Fusion Engineering and Design 197, 2023

[2] L. Piron *et al*, Error Field Control at JET

[3] M.F.F. Nave *et al*, Isotope effects on intrinsic rotation in hydrogen, deuterium and tritium plasmas, Nucl. Fusion 63 044002, 2023

[4] E. Lazzaro *et al*, Error field locked modes thresholds in rotating plasmas, anomalous braking and spin- up, Physics of Plasmas 9, 3906, 2002

[5] L. Piron *et al*, Error Field detection and correction studies towards ITER operation, Nuclear Fusion 64(6), 2024

[6] C. Paz-Soldan *et al*, Non-disruptive error field identification based on magnetic island healing, Nucl. Fusion 62 126007, 2022

[7] L. Piron *et al*, Locked mode detection during error field identification studies, Fusion Engineering and Design 195, 2023

[8] G. Pucella *et al*, Beta-induced Alfvén eigenmodes and geodesic acoustic modes in the presence of strong tearing activity during the current ramp-down on JET, Plasma Phys. Control. Fusion 64, 2022

[9] R.J. Buttery *et al*, Error field experiments in JET, Nucl. Fusion 40 807, 2000

[10] J.T. Scoville *et al.* Nucl. Fusion 31 (1991) 875.

[11] V.S. Marchenko, et al., Nucl. Fusion 56 (2016), 106021.

[12] A.I. Smolyakov, et al., Phys. Rev. Lett. 99 (2007), 055002.

[13] P. Buratti, et al., Nucl. Fusion 45 (2005) 1446.

[14] S.V. Annibaldi, et al., Plasma Phys. Control. Fusion 49 (2007) 475–483.

[15] O. Zimmermann, et al., Coupling of Alfvén-like modes and large 2/1 tearing modes at TEXTOR, in: Proc. 32nd EPS Conf. on Plasma Physics, Tarragona, Spain 29C, 2005. http://epsppd.epfl.ch/Tarragona/pdf/P4059.pdf.

[16] W. Chen, et al., J. Phys. Soc. Japan 79 (2010), 044501.

[17] L. Piron *et al*, Experimental and modelling study of locked mode dynamics prior to disruptions in high performance JET plasmas, 46th EPS Conference on Plasma Physics, 2019

[18] J.A. Wesson 1978 Nucl. Fusion 18 87

[19] D.Ćirić *et al*, Overview of the JET neutral beam enhancement project, Fusion Engineering and Design 82 (2007) 610–618, 2007

[20] D.Ćirić *et al*, Performance of Upgraded JET Neutral Beam Injectors, EFDA–JET–CP(10)07/16, 2010

[21] P.C. de Vries *et al*, Survey of disruption causes at JET, Nucl. Fusion 51 2011 053018, 2015

[22] V. Coccorese *et al*, Design of the New Magnetic Sensors for JET, EFDA–JET–PR(04)041, 2006

[23] G Artaserse *et al*, Refurbishment of JET magnetic diagnostics, NJOC-CPR(18) 19863,

[24] M. Lennholm *et al*,Plasma control at JET, Fusion Engineering and Design 48 (2000) 37–45, 2000

[25] T.M. Biewer *et al*, Expanded Capability of the Edge Charge-Exchange Recombination Spectroscopy System on JET, EFDA–JET–CP(08)03-07, 2008

[26] R C Isler, An overview of charge-exchange spectroscopy as a plasma diagnostic, Plasma phys. Control. Fusion 36 171-208, 1994

[27] Yueqiang Liu *et al*, Modeling plasma toroidal flow profile control via NTV torque with n=2 3-D fields in MAST-U

[28] Cheng Ye et al 2024 Nucl. Fusion 64 016005

[29] Jan Mlynář *et al*, Focus On: JET, EFD-R(07)01, 2007

[30] M Cecconello et al 2023 Plasma Phys. Control. Fusion 65 035013

[31] R.J Buttery *et al*, Stability at High Performance in the MAST Spherical Tokamak, EX/S1-6

[32] J. Wesson, Tokamaks, 3° edition, Clarendon Press, Oxford, 2004

[33] I. H. Hutchinson, Plasma Diagnostics, Massachussetts Institute of Technology, 2° edition, 2002

[34] H. Zohm, Magnetohydrodynamic Stability of Tokamaks, Wiley-VHC, 2014

[35] `https://euro-fusion.org/fusion/history-of-fusion/`

[36] `https://www.iaea.org/newscenter/news/what-is-nuclear-fusion`

[37] `https://www.iter.org/sci/Fusion`

[38] `https://www.iter.org/newsline/-/2567`

[39] `https://en.wikipedia.org/wiki/ITER`

[40] `https://www.iter.org/mach`

[41] `https://wiki.jetdata.eu/open/index.php/Ks5:DDA_Naming_Convention`

[42] `https://www.iter.org/org/team/fst/itpa`

[43] S. Jachmich et al 2022 Nucl. Fusion 62 026012

[44] M. Lehnen et al 2015 Nucl. Fusion 55 123027

[45] Y. Liang *et al*, Mitigation of Type-I ELMs with n = 2 Fields on JET with ITER-like Wall, EFDA–JET–PR(12)51, 2012

[46] L Piron *et al*, Plasma stability in advanced JET ITER-like wall plasmas: first measurements and modelling, EUROFUSION WPJET1-PR(16) 16451, 2016

[47] `https://wiki.jetdata.eu/open/index.php/Ks5:DDA_Naming_Convention`

[48] `https://dvcm.jetdata.eu/documents/144/KS5_DVCM_6mar24.pdf`

[49] Paz-Soldan *et al*, The importance of matched poloidal spectra to error field correction in DIII-D, Phys. Plasmas 21, 072503, 2014

[50] J.T. Scoville et al 1991 Nucl. Fusion 31 875

[51] J.E. Menard et al 2010 Nucl. Fusion 50 045008

[52] S. M. Wolfe *et al*, Nonaxisymmetric field effects on Alcator C-Mod, Phys. Plasmas 12, 056110, 2005

[53] Maraschek M. et al 2013 Measurement and impact of the n=1 intrinsic error field at ASDEX Upgrade 40th EPS Conf. on Plasma Physics, EPS 2013 (Espoo, Finland, 1–5 July 2013) p 4.127

[54] R.J. Buttery et al 1999 Nucl. Fusion 39 1827

[55] R.J. Buttery et al 2000 Nucl. Fusion 40 807

[56] A Kirk et al 2014 Plasma Phys. Control. Fusion 56 104003

[57] Yueqiang Liu et al 2014 Plasma Phys. Control. Fusion 56 104002

[58] Hui-Hui Wang et al 2016 Nucl. Fusion 56 066011

[59] M.J. Schaffer et al 2011 Nucl. Fusion 51 103028

[60] C. Paz-Soldan et al 2014 Nucl. Fusion 54 073013

[61] Y. In et al 2015 Nucl. Fusion 55 043004

[62] M.E. Puiatti et al 2015 Nucl. Fusion 55 104012

[63] P. Zanca et al 2015 Nucl. Fusion 55 043020

[64] R. Fitzpatrick 1993 Nucl. Fusion 33 1049

[65] T. Hender Nuclear Fusion 39 (12 ITER physics basis), 2251-2389, 1999

[66] Felix I Parra and Peter J Catto 2010 Plasma Phys. Control. Fusion 52 045004

[67] Y. Camenen *et al*, Transport of Parallel Momentum Induced by Current-Symmetry Breaking in Toroidal Plasmas, Phys. Rev. Lett. 102, 125001, 2009

[68] R. E. Waltz *et al*, Gyrokinetic simulation of momentum transport with residual stress from diamagnetic level velocity shears, Phys. Plasmas 18, 042504, 2011

[69] T. Sung *et al*, Toroidal momentum transport in a tokamak caused by symmetry breaking parallel derivatives, Phys. Plasmas 20, 042506, 2013

[70] M Barnes and F I Parra 2019 Plasma Phys. Control. Fusion 61 025003

[71] Felix I Parra and Michael Barnes 2015 Plasma Phys. Control. Fusion 57 045002

[72] T Stoltzfus-Dueck 2019 Plasma Phys. Control. Fusion 61 124003

[73] J. Seol, Poloidal flow damping inside transport barriers in a tokamak, Phys. Plasmas 20, 042504, 2013

[74] F L Hinton and M N Rosenbluth 1999 Plasma Phys. Control. Fusion 41 A6

[75] Yueqiang Liu et al 2020 Nucl. Fusion 60 096026